Benzothiadiazole–Dithienopyrrole Donor–Acceptor–Donor and Acceptor–Donor–Acceptor Triads: Synthesis and Optical, Electrochemical, and Charge-Transport Properties

ARTICLE *in* THE JOURNAL OF PHYSICAL CHEMISTRY C · NOVEMBER 2011

Impact Factor: 4.77 · DOI: 10.1021/jp208643k

THE JOURNAL OF PHYSICAL CHEMISTRY C

ARTICLE

pubs.acs.org/JPCC

Benzothiadiazole-Dithienopyrrole Donor−Acceptor−Donor and Acceptor−Donor−Acceptor Triads: Synthesis and Optical, Electrochemical, and Charge-Transport Properties

Lauren E. Polander,[†,§] Laxman Pandey,[†,§] Stephen Barlow,[†,§] Shree Prakash Tiwari,[‡,§,∥] Chad Risko,[†,§] Bernard Kippelen,[‡,§] Jean-Luc Brédas,[†,§] and Seth R. Marder*[,†,§]

[†]School of Chemistry and Biochemistry, [‡]School of Electrical and Computer Engineering, and [§]Center for Organic Photonics and Electronics, Georgia Institute of Technology, Atlanta, Georgia 30332-0400, United States

Supporting Information

ABSTRACT: 2,2′-(Benzo[*c*][1,2,5]thiadiazol-4,7-diyl)-4,4′-dialkyl-bis(4*H*-dithieno[3,2-*b*:2′,3′-*d*]pyrrole) (DTP-BTD-DTP) donor−acceptor−donor (D-A-D) and 4-alkyl-2,6-bis(benzo[*c*][1,2,5]thiadiazol-4-yl)-4*H*-dithieno[3,2-*b*:2′,3′-*d*]pyrrole (BTD-DTP-BTD) acceptor−donor−acceptor (A-D-A) triads, with or without additional alkylation in the DTP 6- or BTD 7-positions, respectively, have been synthesized using Stille coupling reactions, characterized using UV−vis absorption spectroscopy and electrochemistry, modeled using density functional theory calculations, and used as charge-transport materials in field-effect transistors. The choice of alkyl substitution pattern has only minor effects on the optical and redox behavior but can be used to modify the thermal properties and solubility of these compounds. The D-A-D and A-D-A triads show long-wavelength absorption maxima at 566−588 and 517−521 nm, respectively, in solution. These transitions are attributed to excitation from a delocalized HOMO to a BTD-localized LUMO and, accordingly, are bathochromically shifted from those of analogous compounds in which the BDT moieties are replaced by benzene rings (393−417 nm). The triads are oxidized at potentials of +0.01 to +0.37 V vs ferrocenium/ferrocene and are reduced at potentials of −1.95 to −1.74 V, with the D-A-D species being both the most easily oxidized and most easily reduced. Field-effect transistors based on solution-processed films of some of the triads showed p-channel behavior; the highest average hole mobility value measured was 5.9 × 10^{-3} cm^2 V^{-1} s^{-1} for 2,2′-(benzo[*c*][1,2,5]thiadiazol-4,7-diyl)-4,4′-di-*n*-dodecyl-bis(4*H*-dithieno[3,2-*b*:2′,3′-*d*]pyrrole) and was accompanied by an on/off current ratio of ca. 10^3.

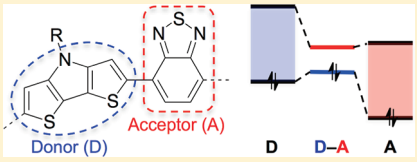

INTRODUCTION

Conjugated species composed of linked donor (D) and acceptor (A) moieties have attracted considerable recent attention for organic electronics applications. In particular, the use of donors (possessing small ionization potentials) and acceptors (with large electron affinities) leads to (i) the possibility of D-to-A charge-transfer-type absorptions in the visible and/or in the near-infrared (NIR) portions of the solar spectrum that can be exploited in photovoltaic cells[1−25] and (ii) the possibility of both hole and electron injection from appropriate electrode materials and, therefore, of ambipolar OFET behavior.[26−36] Although much of the work on D/A materials for OPV and OFET applications has focused on conjugated polymers composed of alternating D and A monomers, there is also increasing interest in D/A small-molecules. As well as serving as models for understanding the fundamental nature of specific D/A interactions in analogous polymers,[37] there are some advantages of directly using small molecules over polymers in device applications. In contrast to polymers, which are typically polydisperse, can be hard to rigorously purify, may contain end groups that interfere with the electronic properties, and which, in some cases, can show considerable batch-to-batch variation in properties, small molecules can be obtained as higher purity single-component materials following chromatography, crystallization, and/or sublimation. This potential for purification, coupled with the possibility of obtaining more ordered crystalline structures, can lead to higher charge-carrier mobility values.[38−40]

Fluorene and carbazole have been largely used as donors in D/A materials, but oligothiophene units, and more recently bridged derivatives, have perhaps been the most widely employed. The alkyl substituents of bridged bithiophene derivatives such as 4,4-dialkyl-4*H*-cyclopenta[2,1-*b*:3,4-*b*′]bithiophene (CPBT), 4,4-dialkyl-4*H*-silolo[3,2-*b*:4,5-*b*′]bithiophene (also known as dithieno[3,2-*b*:2′,3′-*d*]silole, DTS), and 4-alkyl-4*H*-dithieno-[3,2-*b*:2′,3′-*d*]pyrrole (DTP) can be varied to modify solubility and intermolecular packing without introducing large torsions between these units and their neighbors in the conjugated backbone. The planarity of these bridged bithiophenes also leads to lower oxidation potentials than those of unbridged bithiophenes[41−43] and, therefore, stronger donor properties when incorporated into D/A materials.[44]

Many different acceptor units have been exploited in D/A electronic materials, among which [2,1,3]-benzothiadiazole (BTD) has been most widely used. Copolymers of BTD with fluorene,[9,17] silafluorene,[10,11] carbazole,[4,18−20] oligothiophene,[21,22,45]

Received: September 7, 2011
Revised: October 7, 2011
Published: October 10, 2011

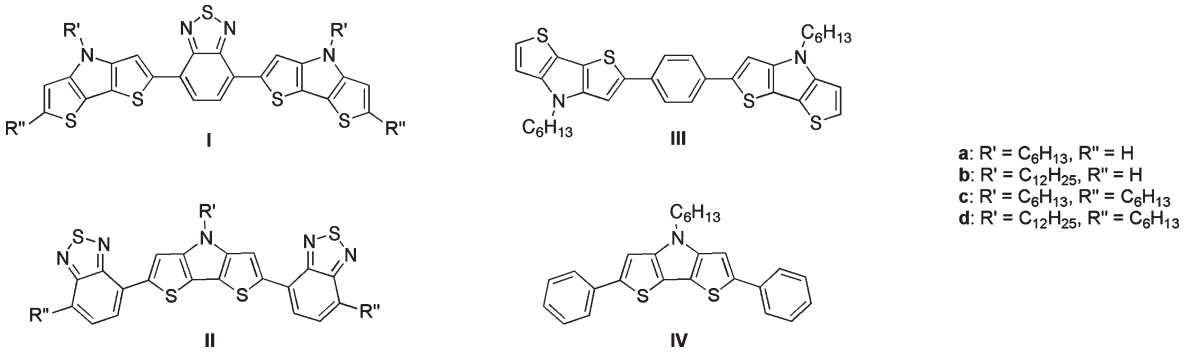

Figure 1. Structures of the D-A-D (**I**) and A-D-A (**II**) triads discussed in this paper, along with two model compounds (**III** and **IV**).

Scheme 1. Preparation of BTD Precursors[a]

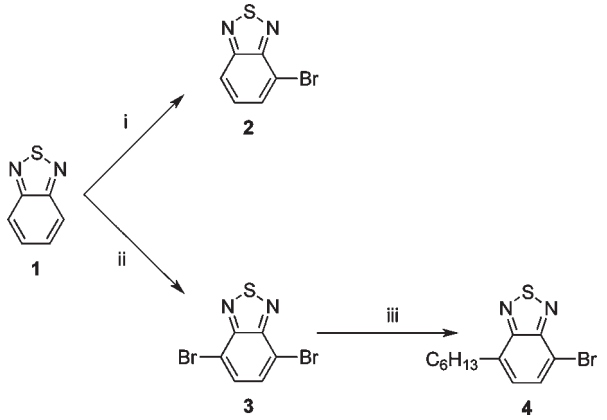

[a] (i) HBr, Br_2 (1 equiv); (ii) HBr, Br_2 (2 equiv); (iii) hexylzinc chloride, $Pd(PPh_3)_4$, THF.

Scheme 2. Preparation of BTD-DTP Triads[a]

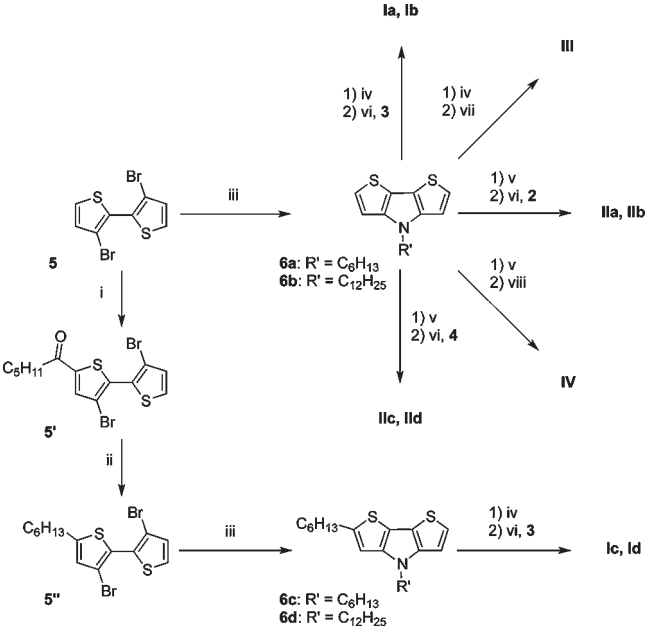

[a] (i) hexanoyl chloride, $AlCl_3$, CH_2Cl_2; (ii) $NaBH_4$, $AlCl_3$; (iii) $R'NH_2$, $Pd_2(dba)_3$, BINAP, NaO^tBu, toluene; (iv) 1) ^{t}BuLi (1 equiv), THF, 2) Bu_3SnCl; (v) 1) ^{t}BuLi (2 equiv), THF, 2) Bu_3SnCl; (vi) $Pd(PPh_3)_2Cl_2$, THF; (vii) $Pd(PPh_3)_2Cl_2$, 1,4-dibromobenzene, THF; (viii) $Pd(PPh_3)_2Cl_2$, 1-bromobenzene, THF.

CPDT,[8,37,46] DTS,[23,3,37] and DTP[21,24,25] groups have been reported; photovoltaic devices made from blends with soluble fullerenes show power conversion efficiencies of up to 6.1%[7] and at least one BTD-based material has been shown to be ambipolar.[37] Small-molecule D-A-D and A-D-A molecules with BTD acceptors and various oligothiophene and planarized oligothiophene donors, including CPDT and DTS have also been investigated;[37,47,48] OFET hole mobility values of 0.17 and 0.006 $cm^2\ V^{-1}\ s^{-1}$ have been reported for vacuum and solution-processed films, respectively, of a bithiophene/BTD D-A-D triad,[49,50] and power conversion efficiencies of up to 3.15% have been observed for OPV cells based on a BTD/terthiophene A-D-A triad.[51] However, the DTP analogues of these small molecules have not been reported. Here we describe the results of a joint experimental and theoretical investigation of the optical, electrochemical, and charge-transport properties of a series of D-A-D and A-D-A small-molecule triads with BTD as the acceptor and DTP as the donor (Figure 1).

RESULTS AND DISCUSSION

Synthesis. The syntheses of compounds of types **I** and **II** are shown in Schemes 1 and 2. Commercially available BTD, **1**, was converted to its 4-bromo and 4,7-dibromo derivatives, **2** and **3**, respectively, according to literature procedures.[52] Compound **3** was converted to **4** by Negishi coupling with hexylzinc chloride (Scheme 1). The DTP precursors **6a** and **6b** were prepared from commercially available 3-bromothiophene via base-catalyzed oxidative homocoupling followed by Buchwald–Hartwig ring closure with the appropriate alkylamine as previously reported.[53−56] The 2-hexyl substituent of **6c** and **6d** was installed through Friedel–Crafts acylation of 3,3′-dibromo-2,2′-bithiophene, **5**, with hexanoyl chloride and aluminum trichloride in dichloromethane, followed by reduction of the resulting ketone using sodium borohydride/aluminum trichloride in refluxing THF to yield the 5-alkylated bithiophene **5′**. Palladium-catalyzed ring closure with the appropriate alkylamine gave the 2-hexyl-DTP precursors, **6c** and **6d** (Scheme 2).[56]

Triads **I** and **II** were prepared from **6** via in situ lithiation and stannylation, followed by palladium-catalyzed cross-coupling. The lithiations were performed using either one or two equivalents of *tert*-butyllithium in THF at −78 °C and the lithiated species was converted to mono or distannyl derivatives by the

Table 1. Decomposition (T_d), Glass Transition (T_g), and Melting (T_m) Temperatures Obtained Using TGA and DSC for the BTD-DTP Triads and Model Compounds

compound	T_d/°C[a]	T_g/°C[b]	T_m/°C[b]
Ia	355	55	173
Ib	360	14	116
Ic	362	*c*	141, 150
Id	367	*c*	53, 135
IIa	389	*c*	202
IIb	384	*c*	107
IIc	378	*c*	160
IId	382	*c*	154
III	368	36	203
IV	315	56	180

[a] Temperature at which 5% weight loss observed using TGA at a heating rate of 5 °C min^{-1}. [b] Glass transition and melting temperatures observed using DSC (second heating, heating rate of 10 °C min^{-1}). [c] No glass transition observed.

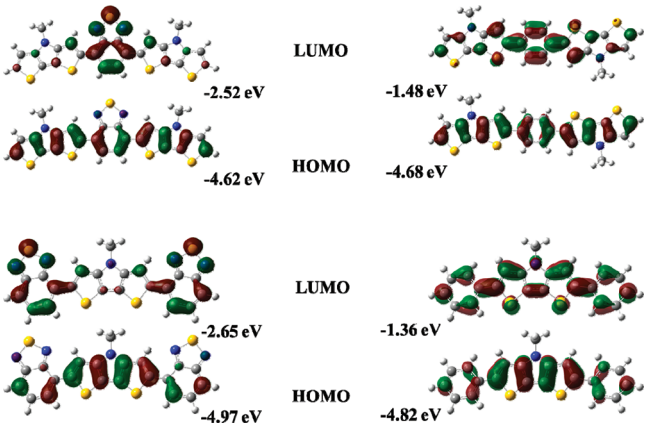

Figure 2. Illustrations of the HOMO and LUMO wave functions and energies of **Ia/b** (top left, orbitals for **Ic/d** are very similar, see Figure S5), **IIa/b** (bottom left, orbitals for **IIc/d** are very similar, see Figure S5), **III** (top-right), and **IV** (bottom-right), as determined at the B3LYP/6-31G** level.

addition of tributylchlorostannane at room temperature. The freshly prepared stannane intermediate was transferred to a flask containing $Pd(PPh_3)_4$ and the appropriate (di)bromo-BTD, **2**−**4**, where they were then stirred at reflux for 18 h. The triads were isolated and purified by silica gel chromatography. The 2,6-diphenyl-substituted DTP model compound, **III**, and the 1,4-phenylene-bridged bis(DTP) derivative, **IV**, were synthesized from Stille coupling of the appropriate (di)stannyl DTP derivative with 1-bromobenzene and 1,4-dibromobenzene, respectively, under similar conditions to those used to obtain triads **I** and **II**.

All of the compounds were characterized by ^{1}H and ^{13}C{^{1}H} NMR spectroscopy, high-resolution mass spectrometry, and elemental analysis. In each case, the compounds with 4-*n*-$C_{12}H_{25}$ substitution on the DTP moiety exhibited increased solubility in $CHCl_3$, CH_2Cl_2, toluene, and THF compared to those with 4-*n*-C_6H_{13} substitution. The use of terminal *n*-hexyl chains also increased the solubility of the materials; however, this solubility improvement was more pronounced in the A-D-A triads, **II**.

The thermal properties of the compounds were investigated by thermogravimetric analysis (TGA, 5 °C min^{-1}, Figure S1, Table 1) and differential scanning calorimetry (DSC, 5 °C min^{-1}, two heating−cooling cycles, Figures S2, S3, and S4). TGA showed decomposition temperatures (defined as that at which 5 wt % loss is observed) above 350 °C for all triads. **Ic** and **Id** exhibited two endothermic transitions on heating (and two corresponding exothermic transitions on cooling), suggesting the formation of liquid-crystalline phases similar to those previously reported for analogous BTD/bithiophene triads:[50] those of **Ic** are seen at 141 and 150 °C on heating and those of **Id** at 53 and 135 °C. The second heating cycle for the **Ia** and **Ib** triads exhibited only features attributed to glass transitions at temperatures, T_g, of 55 and 14 °C, respectively, suggesting films of these compounds can be readily rendered amorphous. Triads **II** each showed single endothermic processes, presumably attributable to melting, at 202, 107, 160, and 154 °C on heating **IIa**, **IIb**, **IIc**, and **IId**, respectively (and corresponding single exothermic events on cooling).

Molecular Geometry and Frontier Orbitals. The neutral ground-state electronic structures obtained at the DFT (B3LYP/6-31G**) level for triads **I** and **II** (with all alkyl groups replaced by methyl groups) are characterized by coplanar DTP and BTD units, whereas torsion angles of 24° and 26° are found between the DTP and benzene rings of the diphenyl-DTP, **III**, and phenylene-bridged bis(DTP), **IV**, model compounds.[57] This is consistent with the expected effects of steric interactions between hydrogen atoms in the 3- and 5-positions of DTP with hydrogen atoms on the benzene rings.

The HOMO and LUMO wave functions (B3LYP/6-31G**) are illustrated for selected compounds in Figure 2.[58] The HOMOs of the triads are delocalized over the DTP rings and the hydrocarbon portion of the BTD rings and can be described as out-of-phase combinations of the HOMOs of the DTP[41] and BTD (see Figure S5) fragments. The LUMOs of **I** and **II**, on the other hand, are rather strongly localized on the BTD unit(s) with similar energies to that of an isolated BTD molecule (see Table S1 and Figure 3); this can be attributed to the larger mismatch in the energies of the BTD and DTP LUMOs than for the HOMOs and to the concentration of the BTD LUMO within its heterocyclic ring, leading to lower coefficients at the point(s) of attachment to DTP. Accordingly, the difference in the HOMO energies of, for example, **Ia** and **IIa** (0.35 eV) is larger than that in the LUMO energies (0.13 eV). The introduction of inductively electron-donating terminal alkyl groups in **Ic/d** and **IIc/d** leads to little difference in the overall shape of the orbitals; however, it destabilizes both HOMO (0.14 and 0.15 eV for **I** and **II** series, respectively) and LUMO (0.08 vs 0.11 eV), the smallest effect being on the **I** LUMO, which is in accord with the localization of that orbital in the center of the molecule, away from the site of alkylation. The relatively delocalized HOMO and localized LUMO of **I** are qualitatively similar to those previously reported for a bis(bithiophene)-BTD D-A-D triad[49] and to those calculated for extended conjugated systems incorporating thiophene-based donors and BTD acceptors, for example, model oligomers for copolymers derived from 2,6-distannyl-DTPs and 5,7-bis(5-bromo-2-thienyl)-BTD.[24]

The HOMOs of the model compounds **III** and **IV** are similar to those of **I** and **II**, respectively, which is consistent with the similar appearance and energies (see Table S1 and Figures 3 and S5) of the DFT HOMOs of isolated BTD and benzene molecules. The LUMOs of **III** and **IV** differ significantly from those of **I** and **II**, respectively, as they are much more significantly

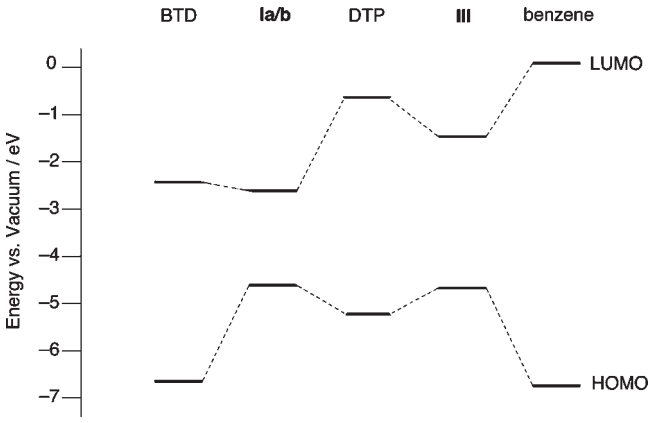

Figure 3. Correlation diagram showing how the DFT frontier orbital energies of the **Ia/b** and **III** compare to those of their constituent building blocks. Note that the orbital energies of **IIa/b** and **IV** are similar to those of **Ia/b** and **III**, respectively (see Table S1).

delocalized over both benzene and DTP and significantly lower in energy than the LUMO of either building block in isolation (but much higher in energy than those of either BTD or the DTP/BTD triads); these trends are consistent with the better match in LUMO energies between DTP and benzene. Both HOMO and LUMO of **III** are similar to the respective orbitals previously reported for the closely related 1,4-(2,2′-bithiophene-5-yl)benzene.[59]

In both the radical cations and radical anions, the structures of **I** and **II** remain coplanar at the DFT level, while the DTP−benzene torsion angles in **III** and **IV** are reduced to 0° and 14° upon oxidation, respectively, and to 2° and 1°, respectively, on reduction. The radical cations of series **I** and **III** and the radical anions of series **II** can, at least in principle, be regarded as organic mixed-valence species[60] in which the hole or electron might be either localized on one end of the molecule or delocalized between two comparable redox centers. The DFT calculations suggest all of the radical ions are symmetric systems both as isolated species or when in a dielectric continuum with a dielectric constant, ε, of 8.93 (to model solvation by dichloromethane), with symmetric geometries and distributions of Mulliken charges (see Figure S6). Given the well-known tendency of conventional DFT to give overdelocalized structures,[61] we also used Hartree−Fock (HF) calculations to investigate the radical-ion geometries. The HF radical-cation structures are fully planar ($\mathbf{I}^{\bullet+}$ and $\mathbf{III}^{\bullet+}$) or nearly planar (angles between DTP and BTD planes of 6 and 4° for $\mathbf{IIa\text{-}b}^{\bullet+}$ and $\mathbf{IIc\text{-}d}^{\bullet+}$, respectively), with the exception of $\mathbf{IV}^{\bullet+}$, which has an increased twist between Ph and DTP rings of of 46°; these results suggest that $\mathbf{I}^{\bullet+}$ and $\mathbf{III}^{\bullet+}$ are symmetrical (class-III-like) species, which is consistent with the similarity of their optical spectra to those of oligothiophene radical cations (see below). The HF radical-anion structures are all planar or almost so (torsion angles of ca. 2° or less) and also point to delocalization in $\mathbf{II}^{\bullet-}$ ions, at least in the gas phase.[62] Both DFT and HF calculations suggest that either oxidation or reduction leads to a more quinoidal pattern of bond lengths, with the DTP−BTD or DTP−benzene bonds shortening by 0.01 to 0.03 Å (see Figure S7 for details), a result consistent with the DTP−BTD/DTP−benzene antibonding character of the HOMOs and DTP−BTD/DTP−benzene bonding character of the LUMOs.

Optical Properties. Electronic spectra of **I**−**IV** were recorded in dilute chloroform solution and as thin films on glass substrates. Representative spectra for the triads are shown in Figure 4; the corresponding absorption maxima, absorptivities, and oscillator strengths are summarized in Table 2. The solution absorption spectra of DTP/BTD triads **I** and **II** exhibit two prominent absorption bands with roughly comparable oscillator strengths in the near-UV/visible range. Both absorptions are observed at lower energy in the D-A-D compounds of type **I** than for the corresponding absorption in A-D-A compounds of type **II**, consistent with previously reported spectra for analogous CPBT/BTD D-A-D and A-D-A triads.[37] Terminal alkylation leads to small bathochromic shifts in the absorption maxima, these shifts being largest in **I**, but as expected, the choice of DTP 4-alkyl group does not significantly affect the spectra.[41,63] The spectra are generally similar to those of previously reported triads with similar structures;[37,47−50] the two bands observed in the absorption spectra of **I** and **II** also resemble those seen for related D/A conjugated polymers, although each band is bathochromically shifted in alternating DTP/BTD conjugated polymers (low-energy bands at ca. 13 000 cm^{-1} in $CHCl_3$)[25] from that in the present small molecules.

Spectra in thin films are fairly similar to those seen in solution with moderate shifts in the absorption maxima (Figure S7). Interestingly, the low-energy absorption maxima of both **Ia** and **Ib** are bathochromically shifted by ca. 700 cm^{-1}, whereas those of **Ic** and **Id** are both bathochromically shifted by ca. 1400 cm^{-1}, suggesting that terminal alkylation can play a significant role in determining intermolecular interactions.

To gain insight into the origin of the spectroscopic properties observed in solution, vertical $S_0 \rightarrow S_n$ excitation energies for isolated molecules were calculated at the time-dependent density functional theory (TD-DFT) level of theory using the B3LYP/6-31G** functional. As shown in Figure 4 and Table 2, the TD-DFT results are in good agreement with the solution and solid-state absorption results, both in terms of excitation energies and oscillator strengths. Although the excitation energies are somewhat underestimated, the differences are within the range typical for the TD-B3LYP method[64,65] and, more importantly, the experimentally observed trends between **Ia/b**, **Ic/d**, **IIa/b**, and **IIc/d** are all reproduced by the calculations.[66] According to the calculations, the strong low-energy transitions in the range 14 200−16 800 cm^{-1} for molecules of both series **I** and **II** correspond to the $S_0 \rightarrow S_1$ transitions and are predominantly HOMO→LUMO one-electron transitions in nature; therefore, they can be regarded as having considerable DTP-to-BTD quadrupolar charge-transfer (CT) character. The variations in experimental and calculated absorption maxima with molecular structure (**I** vs **II** and **a/b** vs **c/d**) can be rationalized by those in the energies of the DFT HOMOs and LUMOs (see above). Compounds of type **I** show similar low-energy maxima to analogous BTD-based D-A-D triads with CPBT donors (17 600−18 100 cm^{-1}),[37,48] these being at lower energy than those for analogues with 5′-alkyl-2,2′-bithiophene-5-yl donors (19 200 cm^{-1});[49,50] this is consistent with previous work showing that CPBT and DTP moieties have similar donor strength to one another and are stronger donors than bithiophenes.[42] The low-energy maxima for the A-D-A derivatives **II** are also similar to those of their CPTD and DTS analogues (19 300 and 19 900 cm^{-1}, respectively).[38,47]

Excitations to the next few excited electronic states are calculated to be very weak, with the strong higher energy (24 700−27 400 cm^{-1}) transitions for compounds of series **I** and **II** corresponding to $S_0 \rightarrow S_5$ and $S_0 \rightarrow S_6$, respectively. In both cases, these transitions largely correspond to excitation from the

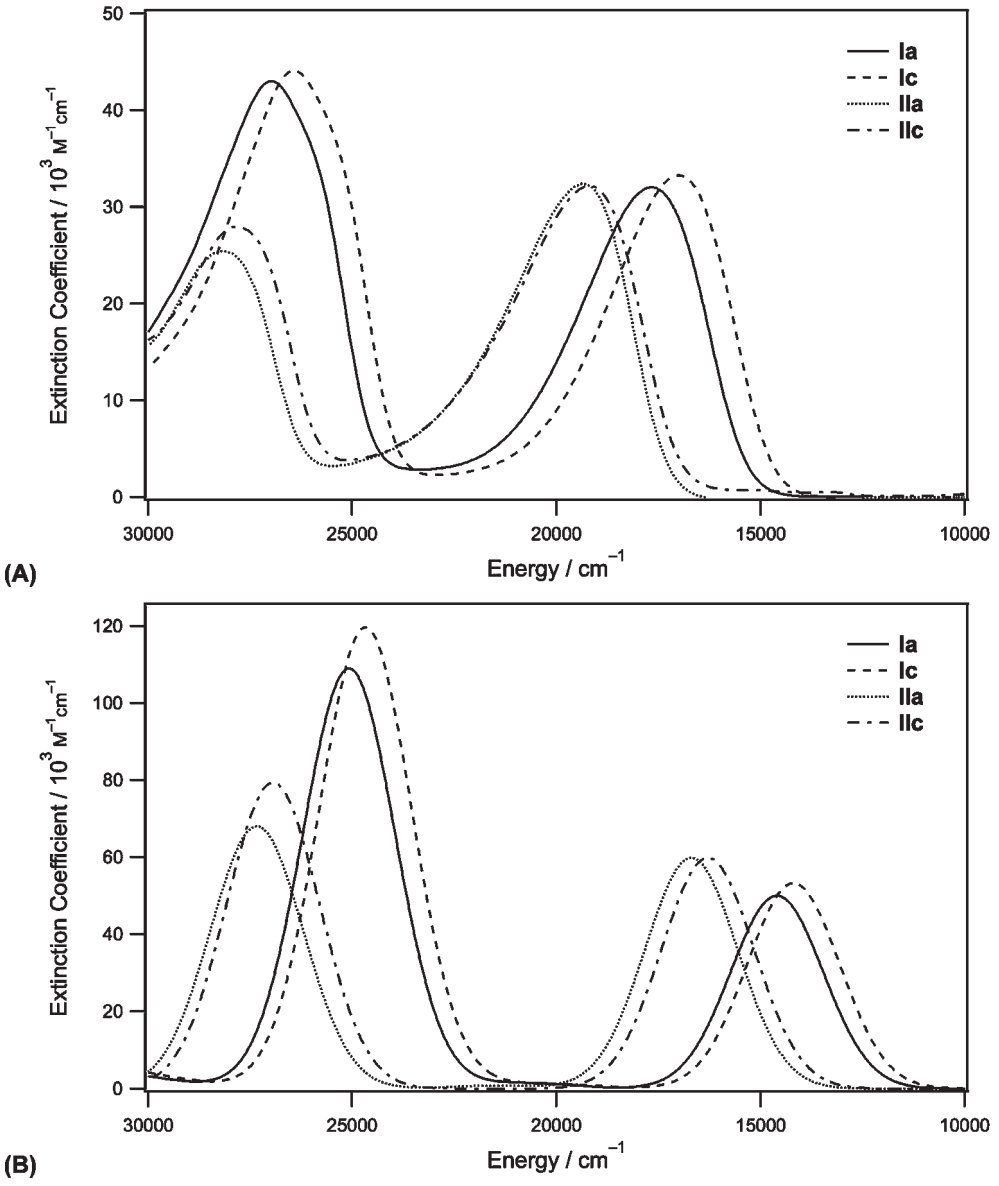

Figure 4. Representative UV−vis spectra of **Ia**, **Ic**, **IIa**, and **IIc** in dilute chloroform solution (A) and calculated spectra at the TD-B3LYP/6-31G**//B3LYP/6-31G** level (B, obtained by applying a Gaussian broadening characterized by a full width at half-maximum of 2660 cm^{-1} to the calculated oscillator strength data).

HOMO to a higher-lying unoccupied molecular orbital (LUMO+1 and LUMO+2 for **I** and **II**, respectively, see Table 2 and SI) with contributions from the LUMO of the DTP fragment and from the BTD group; thus, these transitions do not exhibit the pronounced DTP-to-BTD charge-transfer character of the $S_0 \rightarrow S_1$ transitions.

Replacement of the BTD rings of **I** and **II** with benzene rings in the model compounds **III** and **IV**, respectively, leads to a considerable hypsochromic shift of the lowest energy transition, in agreement with the much higher lying LUMOs calculated (see above) for the model compounds. The TD-DFT calculations indicate that the transitions observed at 24 000−25 400 cm^{-1} can be assigned to $S_0 \rightarrow S_1$ and are largely HOMO → LUMO in character, both relevant orbitals being extensively delocalized along the π backbone. Indeed, the orbitals involved in these transitions are similar to those involved in the $S_0 \rightarrow S_5$ and $S_0 \rightarrow S_6$ transitions of **I** and **II**, respectively, and the transitions are observed at similar energies. The absorption maxima are also observed at similar energies to those of analogous compounds in which the DTP groups are replaced with bithiophene; absorption maxima of 25 600 and 26 800 cm^{-1} have been reported for 1,4-(2,2′-bithiophene-5-yl)benzene[59] and 5,5′-diphenyl-2,2′-bithiophene,[67] respectively, in CH_2Cl_2. The high-energy maxima of compounds of type **II** and the $S_0 \rightarrow S_1$ transition of **IV** are seen at lower energy than the lowest energy absorption of an isolated DTP (32 300 cm^{-1} in CH_2Cl_2[42] and 35 200 cm^{-1} and 79% HOMO → LUMO according to TD-DFT, see SI), reflecting the additional destabilization of the HOMO and stabilization of the relevant empty orbitals by BTD or phenyl contributions. On the other hand, the $S_0 \rightarrow S_1$ transition of **IV** is seen at very similar energy to the lowest energy transition of a 2,2′-bis(DTP), i.e., an analogous compound without the phenylene bridge (24 400 cm^{-1}

Table 2. Absorption Maxima (10^3 cm^{-1}), Absorptivities (10^4 M^{-1} cm^{-1}), and Oscillator Strengths for the Strong UV−vis Absorptions of I−IV in Chloroform along with TD-DFT Values and Assignments (in Italics) and Thin-Film Absorption Maxima[a]

	low-energy band								high-energy band							
	$\bar{\nu}_{max}$			ε_{max}	f		state	CI description (%)[b]	$\bar{\nu}_{max}$			ε_{max}	f		state	CI description (%)[b]
	soln	calc	film		soln	calc			soln	calc	film		soln	calc		
Ia	17.7		17.0	3.21	0.53				27.0		26.5	4.31	0.82			
Ib	17.7	*14.6*	17.0	3.13	0.53	*0.61*	S_1	*H→L (98), H→L+1 (2)*	27.0	*25.1*	26.5	4.20	0.82	*1.33*	S_5	*H→L (2), H→L+1 (96)*
Ic	17.0		15.6	3.32	0.55				26.5		25.7	4.39	0.83			
Id	17.0	*14.2*	15.6	3.39	0.56	*0.65*	S_1	*H→L (98), H→L+1 (2)*	26.5	*24.7*	25.7	4.49	0.87	*1.46*	S_5	*H→L (2), H→L+1 (97)*
IIa	19.3		18.2	3.28	0.55				28.2		28.1	2.57	0.34			
IIb	19.3	*16.8*	18.0	3.34	0.58	*0.73*	S_1	*H→L (82), H→L+2 (2)*	28.2	*27.4*	27.9	2.62	0.35	*0.83*	S_6	*H→L+2 (84)*
IIc	19.2		18.4	3.25	0.60				27.8		27.5	2.82	0.40			
IId	19.2	*16.3*	18.4	3.26	0.60	*0.73*	S_1	*H→L (98)*	27.8	*27.0*	27.5	2.85	0.40	*0.96*	S_6	*H−2→L+1 (2), H→L+2 (93)*
III									24.0	*23.7*	23.8	5.94	*1.24*	*1.75*	S_1	*H→L (99)*
IV									25.4	*25.7*	27.7	4.88	1.05	*1.32*	S_1	*H→L (99)*

[a] TD-DFT values obtained for structures in which the alkyl groups are all replaced by methyl groups at the B3LYP/6-31G** level. The two transitions reported are those seen and/or calculated at $\bar{\nu}_{max}$ < 30 000 cm^{-1} and calculated to have f > 0.05. [b] H and L denote HOMO and LUMO, respectively.

in CH_2Cl_2),[68] presumably due to competition between the effects of an extended π system and disruption of that conjugation by the aromaticity of the phenylene bridge and the reduced coplanarity.

Electrochemistry, Ionization Potentials, Electron Affinities, and Reorganization Energies. The electrochemical properties of **I**−**IV** were investigated using cyclic voltammetry (CV) in dichloromethane/0.1 M tetra-*n*-butylammonium hexafluorophosphate. Representative CV traces are shown in Figure 5 and the redox potentials are summarized in Table 3. The table also includes estimates of solid-state ionization potentials (IPs) and electron affinities (EAs) based on the electrochemical data and values of adiabatic IPs and EAs obtained from DFT calculations for isolated molecules.

I and **II** display reversible features corresponding to both molecular oxidation and reduction. In contrast, the CV traces of **III** and **IV** only display oxidation processes (also reversible) within the accessible solvent window (down to ca. −2.5 V vs $FeCp_2^{+/0}$) under the same conditions, consistent with the absence of the electron-accepting BTD moiety. In the case of the bis(DTP) derivatives **I** and **III**, two well-separated oxidation processes are observed, whereas only one is seen for **II** and **IV**. The current measured for the reduction processes of the bis(BTD) compounds **II** is ca. twice that for the mono-BTD species of type **I**, suggesting two closely overlapping reductions. This is confirmed by differential pulse voltammetry; an example is shown in Figure 5b and shows that the two reductions are separated by ca. 60 mV.

The electrochemical gaps, obtained from the difference between oxidation and reduction potentials, are rather similar to the optical gaps, obtained from the onset of absorption in solution. This suggests that the effects of exciton binding in the excited state are effectively compensated for by solvation of the ions formed in the electrochemical experiments.

The D-A-D molecules, **I**, are ca. 0.25 V more readily oxidized than their A-D-A, **II**, counterparts, in agreement with the results of the DFT calculations, which show HOMO energies ca. 0.35 eV higher (Table S1) and vertical and adiabatic IPs ca. 0.45−0.50 eV lower (Table 3, Table S6), and with the more extended conjugation in these species. The species with terminal alkylation (**Ic**/**d**, **IIc**/**d**) are all ca. 0.1 V more easily oxidized than their nonalkylated analogues (**Ia**/**b**, **IIa**/**b**), consistent with the extension of the HOMO onto the terminal alkylated rings in both D-A-D and A-D-A systems (see above) and with the DFT HOMO energies and IPs. The first oxidation potentials for triads of type **I** are similar to those previously reported for an analogous triad with CPBT donors in place of DTPs (+0.18 V vs $FeCp_2^{+/0}$ in CH_2Cl_2)[48] and lower than those seen for one with 5′-alkyl-2,2′-bithiophene-5-yl donors (ca. +0.46 V in CH_2Cl_2);[50] these results are in line with previous comparisons of the redox properties of CPBT, bithiophene, and DTP derivatives;[42] similarly, the potentials of **III** and **IV** are lower than those of analogues in which bithiophene replaces DTP (E_{ox} = +0.72 V in DMF for 1,4-di(2,2′-bithiophene-5-yl)benzene[69] and $E_{1/2}$ = +0.68 V in CH_2Cl_2 for 5,5′-diphenyl-2,2′-bithiophene[67]).

Despite the presence of two BTD acceptor moieties in the triads of type **II**, these species are oxidized at similar potential to DTPs (irreversibly oxidized with peak potential, E_{ox}, of ca. +0.45 V vs $FeCp_2^{+/0}$ in MeCN),[42] or a 2,6-dialkyl-DTP (+0.23 V in CH_2Cl_2).[42] Also, the triads of type **I** are oxidized at similar potential to a 2,2′-bis(DTP) (E_{ox} = +0.08 V in CH_2Cl_2).[68] Furthermore, replacement of the BTD moieties with benzene rings has little effect on the oxidation potential or DFT IP values,

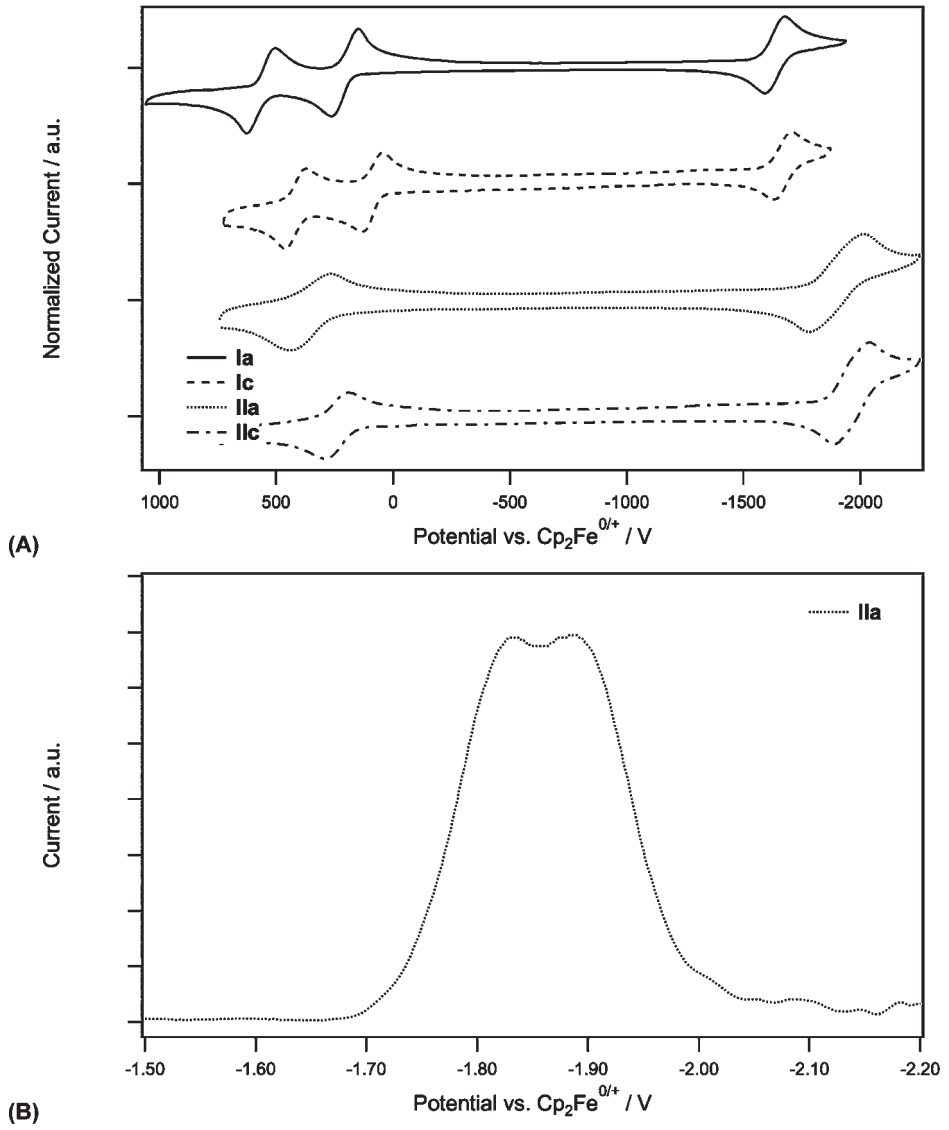

Figure 5. (A) Cyclic voltammograms of **Ia**, **Ic**, **IIa**, and **IIc** in 0.1 M $^{n}Bu_4NPF_6$ in CH_2Cl_2 recorded at a scan rate of 50 mV s^{-1}. Reported potentials are relative to the ferrocenium/ferrocene ($Cp_2Fe^{+/0}$) couple. (B) Reductive differential pulse voltmmogram of **IIa** showing two overlapping reduction processes.

consistent with the similarity of energy and extent of the HOMOs of **III** and **IV** to those of **I** and **II**, respectively, and with the DFT IP values. However, in contrast to the electrochemical data, the DFT adiabatic IPs suggest that **I**−**IV** are much more (0.65−1.30 eV) easily oxidized than DTP in the gas phase (6.70 eV, see SI), in agreement with the higher HOMO energies calculated for the dyads (see above and SI). This is presumably attributable to the influence of solvation on the electrochemical values. Indeed, considerably reduced differences (0.24−0.75 eV) between the adiabatic IPs of **I**−**IV** and DTP are found when evaluated for molecules embedded in a dielectric continuum (dichloromethane, ε = 8.93, see Tables 3 and S6).

The reduction potentials of the BTD-containing triads are observed at −1.74 to −1.95 V vs $FeCp_2^{+/0}$; potentials in the same range have previously been reported for related BTD-based triads[48−51] and for diaryl-BTD derivatives.[70] Moreover, the potentials are similar to that of benzothiadiazole itself, for which $E_{1/2}^{0/-}$ is −1.98 V vs $FeCp_2^{+/0}$, also in dichloromethane,[71] in agreement with the highly BTD-localized nature of the LUMOs (Figure 2). This is broadly consistent with the similar LUMO energies calculated for the triads and BTD (Table S1) but is not reproduced in the DFT-calculated EA values; vertical and adiabatic values of −0.35 and −0.50 eV, respectively, are obtained for BTD, suggesting that the dyads should be ca. 0.9−1.2 eV more readily reduced than the isolated acceptor. The LUMOs and DFT EAs also suggest that the A-D-A triads, **II**, are more easily reduced than the D-A-D species, **I**, while the electrochemical data shows that the opposite is true, at least in solution. Again, solvation effects are likely to play a considerable role in accounting for this discrepancy. Indeed, adiabatic EAs computed by considering a dielectric continuum (dichloromethane, ε = 8.93) for **I** and **II** are similar (ca. −2.7 eV in both systems) and are closer to that calculated for isolated BTD in the same way (−2.37 eV). The introduction of inductively electron-donating terminal alkyl groups leads to slightly less facile reduction, both according to the electrochemical data and the DFT EA values,

Table 3. Electrochemical Potentials (V vs $FeCp_2^{+/0}$),[a] Electrochemically Estimated Solid-State Ionization Potentials and Electron Affinities (eV), and DFT SCF Values for Ionization Potentials, Electron Affinities, and Reorganization Energies for Isolated Molecules (eV)

	experiment							DFT			
	$E_{1/2}^{2+/+}$	$E_{1/2}^{+/0}$	$E_{1/2}^{0/-}$	IP(s)[b]	EA(s)[b]	E_{echem}[c]	E_{op}[d]	IP_{adi}[e]	EA_{adi}[e]	λ_h[f]	λ_e[f]
Ia	+0.47	+0.11	−1.74	4.9	−3.1	1.9	1.9	5.58 (4.63)	−1.38 (−2.71)	0.259	0.194
Ib	+0.46	+0.12	−1.74	4.9	−3.1	1.9	1.9				
Ic	+0.34	+0.01	−1.76	4.8	−3.0	1.8	1.8	5.40 (4.52)	−1.32 (−2.68)	0.257	0.191
Id	+0.34	+0.01	−1.76	4.8	−3.0	1.8	1.8				
IIa	*g*	+0.37	−1.86[h]	5.2	−2.9	2.2	2.1	6.06 (4.93)	−1.60 (−2.75)	0.186	0.151
IIb	*g*	+0.36	−1.88[h]	5.2	−2.9	2.2	2.1				
IIc	*g*	+0.28	−1.94[h]	5.1	−2.9	2.2	2.1	5.88 (4.82)	−1.51 (−2.67)	0.197	0.150
IId	*g*	+0.27	−1.95[h]	5.1	−2.9	2.2	2.1				
III	+0.49	+0.17	*g*	5.0	*i*	*i*	2.7	5.63 (4.66)	−0.52 (−1.81)	0.319	0.314
IV	*g*	+0.31	*g*	5.1	*i*	*i*	2.9	5.99 (4.84)	−0.36 (−1.71)	0.268	0.407

[a] Cyclic Voltammetry in CH_2Cl_2/0.1 M $^nBu_4NPF_6$. [b] Estimated according to $IP(s) = eE_{1/2}^{+/0} + 4.8$ eV and $EA(s) = -(eE_{1/2}^{0/-} + 4.8$ eV).[72] [c] Electrochemical gap, $E_{echem} = e(E_{1/2}^{+/0} - E_{1/2}^{0/-})$. [d] Optical gap for comparison to electrochemical gap estimated from long wavelength onset of absorption in solution. [e] Gas-phase adiabatic IP/EA = SCF energy difference between the relaxed ground-state cation/anion and the ground-state neutral species (obtained for structures in which the alkyl groups are all replaced by methyl groups at the B3LYP/6-31G** level); for vertical IP/EAs, see Table S6. Values in parentheses are calculated for a dielectric continuum with $\varepsilon = 8.93$. [f] Internal reorganization energies for $M_A^{\pm} + M_B = M_A + M_B^{\pm}$ (λ_h or λ_e for + and −, respectively) obtained as sum of the SCF energy difference between cation/anion at the neutral geometry and at cation/anion geometry and that between the neutral species at cation/anion geometry and at neutral geometry. [g] Not observed. [h] For A-D-A species, the observed feature in the cyclic voltammogram corresponds to two closely overlapping corresponding to $\mathbf{II}^{0/-}$ and $\mathbf{II}^{-/2-}$ couples. [i] Could not be determined.

with the effect being larger in the **II** series, which confirms BTD-localized nature of the LUMOs (see Figure 2).

The intramolecular reorganization energies for a self-exchange electron-transfer reaction between the neutral molecules and the corresponding radical cations and anions, λ_h and λ_e, respectively, were also calculated at the B3LYP/6-31G** level (Table 3, see also SI for more details). Indeed, within the framework of Marcus theory, these values are closely related to the barrier to intermolecular hole or electron transport,[73] and, therefore are critical contributors to the charge-carrier mobilities in the materials. Both λ_h and λ_e are calculated to be smallest for triads of type **II** and largest for the model compounds **III** and **IV**. The values for **I** and **II** triads are fairly small compared with those estimated for various other charge-transport materials using similar methods; for example, λ_h values are smaller than those reported for the hole-transport materials *N*,*N*′-diphenyl-*N*,*N*′-bis(3-methylphenyl)-(1,1′-biphenyl)-4,4′-diamine, TPD (0.29 eV),[74] and 2,2′-:5′,2″:5″,2‴:5‴,2⁗:5⁗,2⁗′-sexithiophene (0.30 eV),[75] whereas λ_e values are smaller than that of the electron-transport material tris(8-hydroxyquinolinato)aluminum(III), Alq_3, (0.24 eV).[76] The reorganization energies are, however, larger than those calculated for certain symmetrical planar species with highly delocalized frontier orbitals such as pentacene ($\lambda_h = 0.098$ eV)[77] and 5,6,11,12,17,18-hexaazatrinaphthylene ($\lambda_e = 0.095$ eV).[78]

Radical-Cation Spectra. The radical cations of **Ic**, **IIc**, **III**, and **IV**, were generated in dichloromethane solution using tris(4-bromophenyl)aminium hexachloroantimonate ($E_{1/2}^{+/0} = 0.70$ V vs $FeCp_2^{+/0}$)[79] as an oxidant; the vis-NIR spectra of the resulting solutions are shown in Figure 6 and summarized in Table 4. The spectra all show two conspicuous low-energy transitions consistent with what is seen for the radical cations of other oligothiophene[79,81] and DTP[42,81] derivatives, and with the recently reported spectrum of a BTD-CPDT[38] D-A-D triad.

The vis-NIR spectra of both $\mathbf{III}^{\bullet+}$ and $\mathbf{IV}^{\bullet+}$ show two vibronically structured bands ($\Delta\nu$ = ca. 1500 cm^{-1}). The high and low-energy bands of $\mathbf{IV}^{\bullet+}$ are bathochromically shifted by 6600 and 5100 cm^{-1} relative to those of the unsubstituted *N*-H DTP radical cation (observed in chlorobutane at 77 K);[82] this is somewhat larger than the bathochromic shifts of 2800 and 2400 cm^{-1} seen for high- and low-energy bands on terminal phenylation of terthiophene (3T) radical cations.[80,83] The vis−NIR spectrum of $\mathbf{III}^{\bullet+}$ exhibits an additional bathochromic shift in the high and low-energy peaks of ca. 5000 and 7000 cm^{-1}, respectively, compared to $\mathbf{IV}^{\bullet+}$, which can be attributed to an increase in the conjugation length relative to $\mathbf{IV}^{\bullet+}$; for example, bathochromic shifts in the high and low-energy bands of ca. 2600 and 3500 cm^{-1} are found between 3T and 2,2′:5′,2″:5″,2‴:5‴,2⁗-quaterthiophene (4T) radical cations.[81] Additionally, the significant hypsochromic shift in the low-energy band observed between the radical cation of 5,5′-diphenyl-2,2′-bithiophene (10 700 and 26 800 cm^{-1})[68] and $\mathbf{IV}^{\bullet+}$ is consistent with what is seen between the radical cations of a 2,6-dithienyl-DTP derivative and quaterthiophene analogues.[42,80,81]

The vis-NIR spectra of $\mathbf{Ic}^{\bullet+}$ and $\mathbf{IIc}^{\bullet+}$ exhibit band shapes very similar to those of $\mathbf{III}^{\bullet+}$ and $\mathbf{IV}^{\bullet+}$, respectively, with bathochromic shifts in the high/low-energy peaks of ca. 3600/0 cm^{-1} and 3800/2600 cm^{-1}. Furthermore, the spectrum of $\mathbf{Ic}^{\bullet+}$ closely resembles that of the radical cation of a CPBT-BTD-CPBT triad, for which absorption maxima of 11 300 and 6500 cm^{-1} have been reported.[48]

To gain further insight into the nature of the radical-cation excitations, TD-DFT calculations at the UB3LYP/6-31G** level were performed for $\mathbf{Ic/d}^{\bullet+}$, $\mathbf{IIc/d}^{\bullet+}$, $\mathbf{III}^{\bullet+}$, and $\mathbf{IV}^{\bullet+}$. Note that, in discussing the configurations of the relevant states, we will refer to the SOMO (singly occupied molecular orbital) as the orbital bearing the unpaired electron so that the SOMO[α] spin orbital is the highest orbital occupied by an α spin and the SOMO[β] is vacant, with the neighboring orbitals in energy being referred to as the LUMO and HOMO−1 (see Figure S9). The cations are each calculated to exhibit two ($\mathbf{I}^{\bullet+}$, $\mathbf{III}^{\bullet+}$, $\mathbf{IV}^{\bullet+}$) or more ($\mathbf{II}^{\bullet+}$)

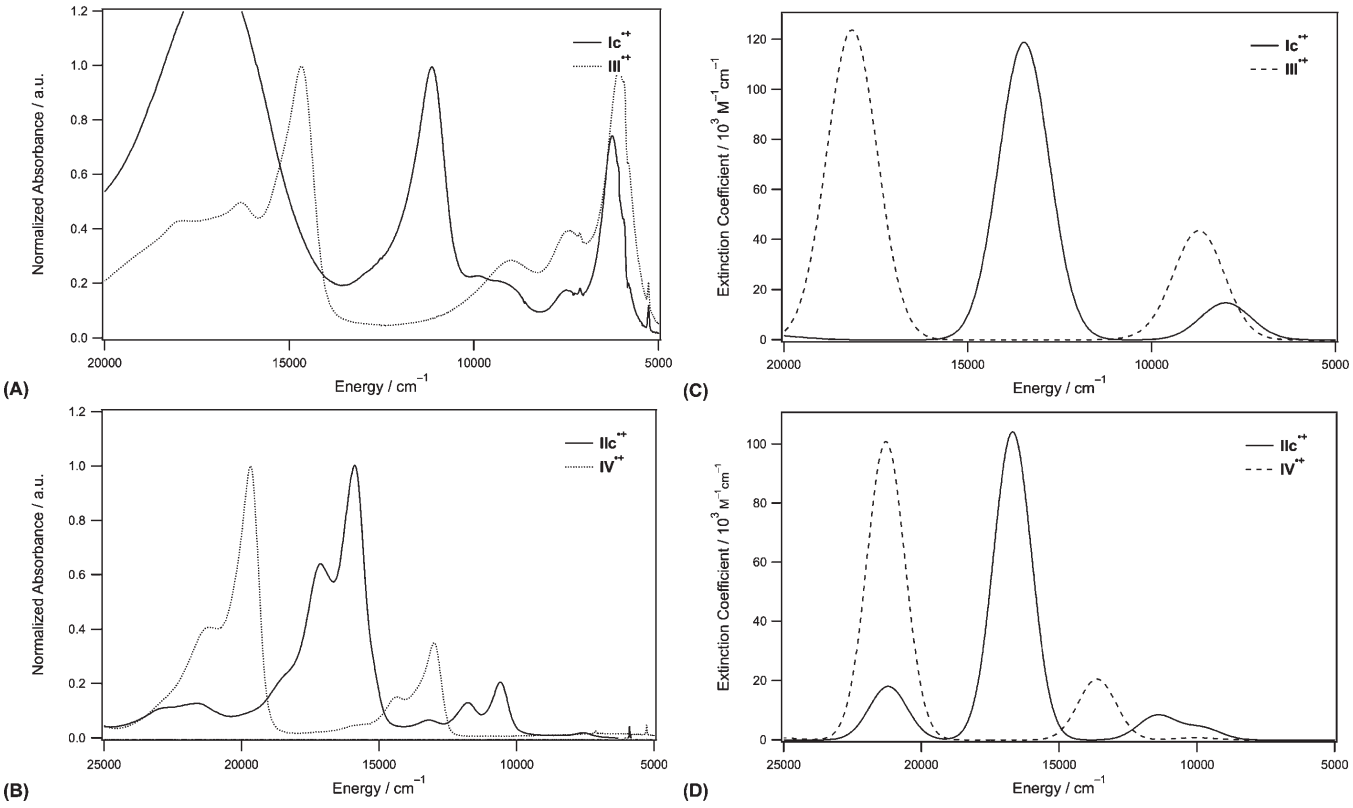

Figure 6. vis−NIR absorption spectra of the radical cations of (A) **Ic** and **III** and of (B) **IIc** and **IV** in dichloromethane. The onset of strong absorption seen at the high-energy edge of the spectrum for **Ic**$^{\bullet+}$ is due to the presence of large excesses of the corresponding neutral species. Calculated spectra of the **Ic**/**d** and **III** (C) and **IIc**/**d** and **IV** (D) radical-cation species at the TD-B3LYP/6-31G**//B3LYP/6-31G** level (obtained by applying a Gaussian broadening characterized by a full width at half-maximum of 1610 cm^{-1} to the calculated oscillator strength data).

moderate to strong absorptions within the vis-NIR region ($\overline{\nu}_{max}$ < 25 000 cm^{-1}), with the lower energy band exhibiting a smaller oscillator strength. These features, and much of the compound-to-compound variation in transition energy, are consistent with experiment, although the transition energies are somewhat overestimated, as are the oscillator strengths for the higher-energy bands. The low-energy transitions of **I**$^{\bullet+}$ and **III**$^{\bullet+}$ are predominantly HOMO−1[β]→SOMO[β] in character (68 and 90%, respectively), with some SOMO[α] → LUMO[α] contribution (31 and 10%, respectively), the HOMO−1, SOMO, and LUMO closely corresponding to the HOMO−1, HOMO, and LUMO, respectively, of the neutral compounds (see Figures S10 and S11). The transitions are qualitatively similar to HOMO−1 → HOMO and HOMO → LUMO electronic excitations of the neutral molecules, respectively. The strong high-energy transitions involve the same configurations but with the SOMO[α]→ LUMO[α] contribution dominating. Three one-electron excitations play an important role in both major transitions calculated for **II**$^{\bullet+}$ and **IV**$^{\bullet+}$: SOMO[α] → LUMO[α], HOMO−2[β] → SOMO[β], and HOMO−1[β] → SOMO[β]. The SOMOs[α/β] essentially correspond to the HOMOs of the neutral molecules, and the HOMO−2[β] of **II**$^{\bullet+}$ corresponds to the HOMO−1 of **II**, whereas the HOMO−1[β] of both species and the HOMO−2[β] of **IV**$^{\bullet+}$ do not closely resemble any of the neutral orbitals (see Figures S12 and S13). In the case of triad **II**$^{\bullet+}$, an additional weak (f = 0.05) transition, again involving contributions from the same three one-electron excitations, is calculated for **II**$^{\bullet+}$ at 9800 cm^{-1}; this may correspond to the weak feature seen in the experimental spectrum at ca. 7000 cm^{-1} or may overlap with the stronger low-energy transition. An additional moderately strong (f = 0.22) higher-energy transition (with a complex CI description) is also calculated for **II**$^{\bullet+}$ at 21 200 cm^{-1} and presumably corresponds to the feature measured at ca. 22 000 cm^{-1}.

OFET Behavior. The electrical properties of the triads were investigated by fabricating and testing field-effect transistor devices using solution-processing techniques. Bottom-gate and top-contact geometry devices were fabricated on heavily n-doped silicon substrates, which also serve as the gate electrodes, with 200 nm thick thermally grown SiO_2 as the gate dielectric. The source and drain electrodes were gold. No n-channel behavior was detected, which is not very surprising given the moderate solid-state electron affinities estimated for these materials (see Table 3) and the use of gold electrodes. However, as shown in Table 5, several of the triads exhibited p-channel behavior with moderate mobility values and on/off current ratios, the variation presumably being related to differences in packing and film morphology. Interestingly, the two species showing the highest mobility values and that are most easily turned on (**Ia** and **Ib**) are those that DSC studies suggest form amorphous films. While falling short of the best values achieved for solution-processed small-molecule oligothiophenes (up to 0.1 cm^2 V^{-1} s^{-1})[75−77] and for DTP-based small molecules (0.01 cm^2 V^{-1} s^{-1}),[84] the mobility values are similar to the best achieved for related compounds such as the BTD/bithiophene triads studied by Sonar et al.[50,58]

Table 4. Absorption Maxima (10^3 cm^{-1}), Absorptivities (10^4 M^{-1} cm^{-1}), and Oscillator Strengths for the Strong vis−NIR Absorptions of I−IV Radical Cations in Dichloromethane along with TD-DFT Values and Assignments (in Italics)[a]

	low-energy band								high-energy band							
	$\bar{\nu}_{max}$				f				$\bar{\nu}_{max}$				f			
	soln	calc	ε_{max}		soln	calc	state	CI description (%)[b]	soln	calc	ε_{max}		soln	calc	state	CI description (%)[b]
$\mathbf{Ic}^{\bullet+}$	6.2	8.0	e	e	0.18	D_1	$S_\alpha \rightarrow L_\alpha$ (31), $H-1_\beta \rightarrow S_\beta$ (68)	11.1	13.5	e	e	1.45	D_4	$S_\alpha \rightarrow L_\alpha$ (63), $H-1_\beta \rightarrow S_\beta$ (30)
$\mathbf{IIc}^{\bullet+}$	10.5	*11.4*[c]	1.9	0.10	*0.10*[c]	D_2	$S_\alpha \rightarrow L_\alpha$ (21), $H-2_\beta \rightarrow H-1_\beta$ (51), $H-1_\beta \rightarrow S_\beta$ (22)	15.9	*16.7*[d]	6.0	0.58	*1.27*[d]	D_4	$S_\alpha \rightarrow L_\alpha$ (55), $H-2_\beta \rightarrow S_\beta$ (6), $H-1_\beta \rightarrow S_\beta$ (23)
$\mathbf{III}^{\bullet+}$	6.1	8.7	6.0	0.54	0.53	D_1	$S_\alpha \rightarrow L_\alpha$ (10), $H-1_\beta \rightarrow S_\beta$ (90)	14.7	*18.1*	6.1	0.88	*1.51*	D_5	$S_\alpha \rightarrow L_\alpha$ (82), $H-1_\beta \rightarrow S_\beta$ (11)
$\mathbf{IV}^{\bullet+}$	13.1	*13.6*	2.1	0.15	*0.25*	D_2	$S_\alpha \rightarrow L_\alpha$(16), $H-2_\beta \rightarrow H-1_\beta$ (58), $H-1_\beta \rightarrow S_\beta$ (23)	19.7	*21.3*	6.1	0.49	*1.23*	D_7	$S_\alpha \rightarrow L_\alpha$ (76), $H-2_\beta \rightarrow H-1_\beta$ (9), $H-1_\beta \rightarrow S_\beta$ (7)

[a] TD-DFT values obtained for structures in which the alkyl groups are all replaced by methyl groups at the B3LYP/6-31G** level. The two transitions reported are those seen and/or calculated at $\bar{\nu}_{max} <$ 25 000 cm^{-1} and calculated to have $f \geq 0.05$. [b] H, S, and L denote HOMO, SOMO, and LUMO, respectively. [c] Excitation to D_1 is calculated at 9800 cm^{-1} ($f = 0.05$) with CI description: $S_\alpha \rightarrow L_\alpha$ (5), $H-2_\beta \rightarrow H-1_\beta$ (41), $H-1_\beta \rightarrow S_\beta$ (52). [d] Excitation to D_9 is calculated at 21 200 cm^{-1} ($f = 0.22$) with CI description: $S_\alpha \rightarrow L_\alpha$ (11), $S_\alpha \rightarrow L+2_\alpha$ (12), $H-3_\beta \rightarrow L_\beta$ (11), $H-1_\beta \rightarrow L+1_\beta$ (21). [e] Could not be determined.

Table 5. Saturation Hole Mobility Values, Threshold Voltages, and Current on/off Ratios for OFETs Based on DTP-BTD Triads[a]

	μ_h[a]/cm^2 V^{-1} s^{-1}	V_{TH}/V	I_{on}/I_{off}
Ia	1.0 (±0.2) × 10^{-3}	7.9 (±2.0)	1 × 10^2
Ib	5.9 (±1.9) × 10^{-3}	9.5 (±3.3)	1 × 10^3
Ic	2.2 (±0.1) × 10^{-4}	0.2 (±0.8)	3 × 10^3
Id	2.5 (±0.2) × 10^{-4}	−0.7 (±1.4)	4 × 10^3
IIa	*b*	*b*	*b*
IIb	6.6 (±1.6) × 10^{-5}	−11.0 (±4.4)	2 × 10^2
IIc	*b*	*b*	*b*
IId	*b*	*b*	*b*

[a] Average values are calculated based on 3 to 6 devices with $W = 1200$ and $L = 100\ \mu$m from a single substrate. [b] No measurable OFET behavior.

SUMMARY

D-A-D and A-D-A triads based on DTP donors and BTD acceptors have been synthesized, characterized using UV−vis absorption and electrochemistry, and studied using (TD)DFT calculations. The HOMOs are delocalized over both DTP and BTD units, resembling those of model compounds in which benzene rings replace the BTD moieties and those of oligothiophenes, the local HOMO of the BTD building block being sufficiently high in energy for effective overlap with the DTP HOMO. On the other hand, the LUMOs are largely localized on the BTD groups. Accordingly, some properties, such as the low-energy absorptions of the neutral species, where HOMO-to-LUMO excitation is accompanied by significant DTP-to-BTD charge transfer, resemble those of other donor−acceptor systems, whereas other properties, such as the low-energy absorptions of the radical cations, where the excitation occurs predominantly from a delocalized filled orbital to the delocalized SOMO (corresponding to the HOMO of the neutral molecule), resemble those of other more delocalized systems, such as the benzene-containing model compounds and oligothiophenes.

Some of the triads exhibit moderate average hole mobility values (up to 5.9 × 10^{-3} cm^2 V^{-1} s^{-1}) in OFETs. Although higher mobility values have been observed in solution-processed p-channel OFETs based on other materials, the present values, coupled with the low-energy absorptions exhibited by the triads, do suggest possible use as donor materials for photovoltaic applications.[85]

EXPERIMENTAL METHODS

Materials. Starting materials were reagent grade and were used without further purification unless otherwise indicated. Solvents were dried by passing through columns of activated alumina (toluene, CH_2Cl_2) or by distillation from Na/benzophenone (THF) or were obtained as anhydrous grade from Acros Organics.

Characterization. Chromatographic separations were performed using standard flash column chromatography methods using silica gel purchased from Sorbent Technologies (60 Å, 32−63 μm). ^{1}H and ^{13}C{^{1}H} NMR spectra were obtained with chemical shifts referenced to $CDCl_3$ using the ^{1}H resonance of the residual protio solvent signal or the ^{13}C resonance of the deuterated solvent, respectively. EI and FAB mass spectra were recorded on a VG Instruments 70SE or a Micromass AutoSpec. Differential scanning calorimetry (DSC) was carried out under

nitrogen on a TA Instruments Q200 (scanning rate of 5 °C min^{-1}). Thermogravimetric analysis (TGA) was carried out using a Netzsch STA 449 C Jupiter (heating rate of 5 °C min^{-1}). Electrochemical measurements were carried out under nitrogen in dry deoxygenated 0.1 M tetra-*n*-butylammonium hexafluorophosphate in dichloromethane using a conventional three-electrode cell with a glassy carbon working electrode, platinum wire counter electrode, and a Ag wire coated with AgCl as a pseudoreference electrode. Potentials were referenced to ferrocenium/ferrocene by using decamethylferrocene (−0.55 V vs ferrocenium/ferrocene) as an internal reference. Cyclic voltammagrams were recorded at a scan rate of 50 mV s^{-1}. UV−vis−NIR spectra were recorded in 1 cm cells using a Varian Cary 5E spectrometer. GCMS data were acquired on an Agilent 5790 GC/6850 MS. Elemental analyses were performed by Atlantic Microlabs.

Computational Methodology. Calculations for the isolated molecular neutral, radical-cation, and radical-anion states were carried out with density functional theory (DFT), using the generalized gradient approximation B3LYP functional,[86−88] in conjunction with a 6-31G**[89−91] basis set. Due to the tendency of DFT methods to overestimate the extent of wave function delocalization,[61,92] geometries were also optimized at the Hartree−Fock (HF/6-31G**) level. All alkyl side chains were replaced with methyl groups to reduce the computational cost. Low-lying singlet excited states were evaluated at the neutral ground-state geometries using time-dependent density functional theory (TDDFT) at the B3LYP/6-31G** level of theory. Since TD-DFT-B3LYP is known to have problems giving the correct description of charge-transfer excitations,[93,94] long-range-corrected CAM-B3LYP[95] and ωB97X[93] functionals (with ω-values of 0.33 and 0.30 $bohr^{-1}$, respectively, for the long-range correction parameters) were also used to investigate the $S_0 \rightarrow S_n$ transitions. Additionally, TD-UB3LYP/6-31G** was employed to evaluate the vertical transition energies of the radical-cation structures. Solvation effects on the IPs and EAs were evaluated with the polarization continuum model[96] taking into account the dielectric constant of dichloromethane, $\varepsilon = 8.93$. All calculations were performed using the Gaussian (03 revision E.01[97] and 09 revision A.02[98]) suites of programs.

Fabrication of Thin Film Transistors. Device measurements were performed on bottom-gate OFETs fabricated on heavily doped n-type silicon substrates (which also serve as gate electrodes) with 200 nm thick thermally grown SiO_2 as the gate dielectric. Ti/Au (10 nm/100 nm) metallization on the backside of the substrate was done to enhance the gate electrical contact. First, the substrates were cleaned by O_2 plasma for 3 min, to improve film formation by increasing the hydrophilicity of the SiO_2 surface. The capacitance density of the SiO_2 layer was 16.2 nF cm^{-2}. A thin layer of organic semiconductor was formed on the substrates by spin coating with a solution (12 mg/mL) in chloroform. Au (ca. 75 nm) was deposited through a shadow mask to act as top source/drain electrode. The devices were annealed at 130 °C for 30 min before device characterization.

Synthetic Procedures. *4-Bromo-7-hexylbenzo[c][1,2,5]-thiadiazole (**4**).* A solution of hexylmagnesium bromide (9.66 g, 0.051 mol) in dry diethyl ether (25 mL, 2 M) was added to a solution of zinc chloride (6.18 g, 0.061 mol) in dry THF (60 mL, 1 M) at 0 °C, and the mixture was stirred for 1 h at room temperature. The resultant hexylzinc chloride solution was added to a mixture of 4,7-dibromobenzo[*c*][1,2,5]thiadiazole (15.0 g, 0.051 mol), tetrakis(triphenylphosphine) palladium (0.295 g, 0.255 mmol), and dry THF (25 mL) at 0 °C. The reaction mixture was stirred for 2 d after which an additional aliquot of hexylzinc chloride (9.49 g, 0.025 mol) was added, and the mixture was stirred at room temperature for 20 h while being monitored by GCMS. Upon completion, the reaction mixture was diluted with dichloromethane, washed with saturated aqueous ammonium chloride solution, and dried over anhydrous sodium sulfate. The combined organic washes were filtered through a plug of Celite, and the filtrate was concentrated via rotary evaporation. The crude product was purified by flash chromatography (silica gel, 1:1 hexane:toluene). The solvent was removed under reduced pressure. The product was further purified by bulb-to-bulb distillation at 135 °C/0.05 Torr (4.03 g, 0.013 mmol, 26%). ^{1}H NMR (400 MHz, $CDCl_3$) δ 7.72 (d, J = 7.6 Hz, 1H), 7.21 (d, J = 7.6 Hz, 1H), 3.05 (t, J = 7.6 Hz, 2H), 1.75 (quint., J = 7.6 Hz, 2H), 1.39−1.28 (m, 6H), 0.86 (t, J = 7.0 Hz, 3H). ^{13}C{^{1}H} NMR (100 MHz, $CDCl_3$) δ 154.7, 153.4, 136.0, 132.0, 127.8, 111.1, 32.0, 31.6, 29.6, 29.1, 22.6, 14.1. HRMS (EI): m/z calcd for $C_{12}H_{15}BrN_2S$ (M^+): 298.0139. Found: 298.0163. Anal. Calcd. for $C_{12}H_{15}BrN_2S$: C, 48.17; H, 5.05; N, 9.36. Found: C, 48.30; H, 5.08; N, 9.54.

*1-(3,3′-Dibromo-2,2′-bithiophen-5-yl)hexan-1-one (**5′**).* In a dry flask, a mixture of 3,3′-dibromo-2,2′-bithiophene (15.0 g, 46.3 mmol) and aluminum trichloride (7.41 g, 55.6 mmol) was purged with nitrogen. After 20 min, dry dichloromethane (460 mL) was added, and the solution was cooled to 0 °C before hexanoyl chloride (7.48 g, 55.6 mmol) was added dropwise over 5 min. The mixture was stirred at room temperature for 3 h. Upon completion, the reaction mixture was quenched with water, extracted with dichloromethane, and dried over anhydrous sodium sulfate. The combined dichloromethane washes were concentrated via rotary evaporation and the crude product was purified by flash chromatography (silica gel, 1:1 hexane:dichloromethane). The solvent was removed under reduced pressure. The product was collected as a yellow oil (17.3 g, 41.0 mmol, 89%). ^{1}H NMR (400 MHz, $CDCl_3$) δ 7.62 (s, 1H), 7.44 (d, J = 5.4 Hz, 1H), 7.09 (d, J = 5.4 Hz, 1H), 2.85 (t, J = 7.4 Hz, 2H), 1.74 (quint., J = 7.3 Hz, 2H), 1.35 (m, 4H), 0.90 (t, J = 7.0, 3H). ^{13}C{^{1}H} NMR (100 MHz, $CDCl_3$) δ 192.4, 143.8, 136.7, 134.4, 131.2, 128.2, 128.1, 113.0, 112.4, 39.0, 31.4, 24.2, 22.4, 13.9. HRMS (EI): m/z Calcd for $C_{14}H_{14}Br_2OS_2$ (M^+): 419.8853. Found: 418.8859. Anal. Calcd. for $C_{14}H_{14}Br_2OS_2$: C, 39.83; H, 3.34. Found: C, 39.94; H, 3.26.

*3,3′-Dibromo-5-hexyl-2,2′-bithiophene (**5″**).* In a dry flask, aluminum trichloride (11.9 g, 89.5 mmol) was added slowly to a solution of sodium borohydride (5.66 g, 0.149 mol) in dry THF (300 mL). A solution of 1-(3,3′-dibromo-2,2′-bithiophen-5-yl)-hexan-1-one (12.6 g, 29.8 mmol) in dry THF (10 mL) was added, and the mixture was stirred at reflux for 20 h. Upon completion, the reaction mixture was quenched with cold water, extracted with ethyl acetate, and dried over anhydrous sodium sulfate. The combined ethyl acetate washes were concentrated via rotary evaporation, and the crude product was purified by flash chromatography (silica gel, hexanes). The solvent was removed under reduced pressure. The product was collected as a yellow oil (7.31 g, 17.9 mmol, 60%). ^{1}H NMR (500 MHz, $CDCl_3$) δ 7.35 (d, J = 5.5 Hz, 1H), 7.04 (d, J = 5.5 Hz, 1H), 6.75 (d, J = 5.5 Hz, 1H), 2.77 (t, J = 7.8 Hz, 2H), 1.67 (quint., J = 7.7 Hz, 2H), 1.39−1.24 (m, 6H), 0.89 (t, J = 6.8, 3H). ^{13}C{^{1}H} NMR (125 MHz, $CDCl_3$) δ 147.95, 130.70, 129.51, 127.63, 127.10, 125.84, 112.15, 111.47, 31.47, 31.03, 30.19, 28.71, 22.52, 14.05. HRMS (EI) m/z Calcd for $C_{14}H_{16}Br_2S_2$ (M^+): 405.9060. Found: 405.9065.

*2,4-Dihexyl-4H-dithieno[3,2-b:2′,3′-d]pyrrole (**6c**).* A solution of 3,3′-dibromo-5-hexyl-2,2′-bithiophene (5.00 g, 12.3 mmol), sodium *tert*-butoxide (3.53 g, 36.7 mmol), tris(dibenzylideneacetone)

dipalladium ($Pd_2(dba)_3$; 0.280 g, 0.306 mmol), and BINAP (0.763 g, 1.23 mmol) in dry toluene (25 mL) was purged with nitrogen. After 20 min, 1-hexylamine (1.24 g, 12.3 mmol) was added, and the mixture was stirred for 8 h at 120 °C. After cooling, the reaction mixture was filtered through silica gel eluting with 2% ethylacetate in hexanes. The crude product was purified by flash chromatography (silica gel, 1:5 dichloromethane in hexanes). The solvent was removed under reduced pressure. The product was collected as a yellow oil (3.64 g, 10.5 mmol, 85%). ^{1}H NMR (400 MHz, $CDCl_3$) δ 7.03 (d, J = 5.3 Hz, 1H), 6.95 (d, J = 5.3 Hz, 1H), 6.69 (s, 1H), 4.12 (t, J = 7.1 Hz, 2H), 2.86 (t, J = 7.6 Hz, 2H), 1.82 (quint., J = 7.2 Hz, 2H), 1.71 (quint., J = 7.5 Hz, 2H), 1.42−1.22 (m, 12H), 0.88 (t, J = 7.0, 3H), 0.85 (t, J = 7.1 Hz, 3H). ^{13}C{^{1}H} NMR (100 MHz, $CDCl_3$) δ 144.17, 144.04, 143.50, 121.56, 114.84, 112.20, 110.85, 108.26, 47.31, 31.74, 31.60, 31.49, 31.42, 30.36, 28.76, 26.66, 22.59, 22.51, 14.09, 14.00. HRMS (EI): m/z Calcd for $C_{20}H_{29}NS_2$ (M^+): 347.1741. Found: 347.1734. Anal. Calcd. for $C_{20}H_{29}NS_2$: C, 69.11; H, 8.41; N, 4.03. Found: C, 69.15; H, 8.52; N, 4.02.

*4-Dodecyl-2-hexyl-4H-dithieno[3,2-b:2′,3′-d]pyrrole (**6d**).* A solution of 3,3′-dibromo-5-hexyl-2,2′-bithiophene (4.00 g, 9.80 mmol), sodium *tert*-butoxide (2.83 g, 29.4 mmol), tris-(dibenzylideneacetone) dipalladium ($Pd_2(dba)_3$; 0.224 g, 0.245 mmol), and BINAP (0.610 g, 0.980 mmol) in dry toluene (20 mL) was purged with nitrogen. After 20 min 1-dodecylamine (1.82 g, 9.80 mmol) was added, and the mixture was stirred for 12 h at 120 °C. After cooling, the reaction mixture was filtered through silica gel eluting with 2% ethyl acetate in hexanes. The crude product was purified by flash chromatography (silica gel, 10% dichloromethane in hexanes). The solvent was removed under reduced pressure. The product was collected as a yellow oil (1.45 g, 3.36 mmol, 34%). ^{1}H NMR (400 MHz, $CDCl_3$) δ 7.03 (d, J = 5.3 Hz, 1H), 6.95 (d, J = 5.3 Hz, 1H), 6.69 (s, 1H), 4.11 (t, J = 7.1 Hz, 2H), 2.85 (t, J = 7.4 Hz, 2H), 1.82 (quint., J = 7.0 Hz, 2H), 1.70 (p, J = 7.5 Hz, 2H), 1.40−1.22 (m, 24H), 0.88 (t, J = 7.0, 3H), 0.86 (t, J = 7.0 Hz, 3H). ^{13}C{^{1}H} NMR (100 MHz, $CDCl_3$) δ 144.17, 144.04, 143.49, 121.55, 114.84, 112.19, 110.85, 108.26, 47.30, 31.90, 31.74, 31.60, 31.49, 30.38, 29.60, 29.57, 29.47, 29.44, 29.33, 29.24, 28.77, 26.99, 22.68, 22.59, 14.11, 14.09. HRMS (EI): m/z Calcd for $C_{26}H_{41}NS_2$ (M^+): 431.2680. Found: 431.2693. Anal. Calcd. for $C_{26}H_{41}NS_2$: C, 72.33; H, 9.57; N, 3.24. Found: C, 72.45; H, 9.72;N, 3.27.

*General Procedure for D-A-D Triads, **I** and **III**.* A 0.1 M solution of the appropriate DTP **6** (1 equiv) in dry THF was cooled to −78 °C under nitrogen. After 20 min, *tert*-butyllithium (1 equiv) was added dropwise, and the mixture was stirred for 2.5 h at −78 °C. Tributyltin chloride (1 equiv) was added dropwise and the mixture was allowed to warm to room temperature and stir for 1 h. This solution was transferred into a separate flask containing *trans*-dichlorobis(triphenylphosphine)palladium (5 mol %) and a 0.1 M solution of **3** (0.45 equiv) in dry THF; the resulting solution was heated to reflux for 19 h. After cooling, the reaction mixture was quenched with water, extracted with diethyl ether, and dried over anhydrous sodium sulfate. The combined ether washes were concentrated via rotary evaporation.

*2,2′-(Benzo[c][1,2,5]thiadiazol-4,7-diyl)-4,4′-di-n-hexyl-bis-(4H-dithieno[3,2-b:2′,3′-d]pyrrole) (**Ia**).* The crude product was purified by flash chromatography (silica gel, 1:1 hexanes/toluene). The product was recrystallized from isopropanol and collected as a dark purple solid (1.29 g, 3.44 mmol, 38%). ^{1}H NMR (400 MHz, $CDCl_3$) δ 8.18 (s, 2H), 7.66 (s, 2H), 7.15 (d, J = 5.3 Hz, 2H), 6.93 (d, J = 5.3 Hz, 2H), 4.12 (t, J = 7.0 Hz, 4H), 1.86 (quint., J = 7.1 Hz, 4H), 1.36−1.23 (m, 12H), 0.86 (t, J = 7.0 Hz, 6H). ^{13}C{^{1}H} NMR (100 MHz, $CDCl_3$) δ 152.41, 145.70, 145.63, 136.84, 126.05, 124.25, 123.90, 115.12, 114.83, 112.04, 110.90, 47.19, 31.41, 30.34, 26.65, 22.52, 14.05. HRMS (EI): m/z Calcd for $C_{34}H_{34}N_4S_5$ (M^+): 658.1387. Found: 658.1361. Anal. Calcd. for $C_{34}H_{34}N_4S_5$: C, 61.97; H, 5.20; N, 8.50. Found: C, 61.77; H, 5.13; N, 8.44.

*2,2′-(Benzo[c][1,2,5]thiadiazol-4,7-diyl)-4,4′-di-n-dodecyl-bis-(4H-dithieno[3,2-b:2′,3′-d]pyrrole) (**Ib**).* The crude product was purified by flash chromatography (silica gel, 4:1 hexanes/toluene then 2:1 hexanes/toluene). The product was recrystallized from isopropanol and collected as a dark purple solid (0.580 g, 0.920 mmol, 37%). ^{1}H NMR (400 MHz, $CDCl_3$) δ 8.27 (s, 2H), 7.80 (s, 2H), 7.17 (d, J = 5.3 Hz, 2H), 6.99 (d, J = 5.3 Hz, 2H), 4.23 (t, J = 7.0 Hz, 4H), 1.91 (quint., J = 6.8 Hz, 4H), 1.27 (m, 36H), 0.84 (t, J = 6.8 Hz, 6H). ^{13}C{^{1}H} NMR (100 MHz, $CDCl_3$) δ 152.9, 146.1, 146.0, 137.2, 126.6, 124.9, 124.4, 115.6, 115.2, 112.4, 111.2, 47.6, 32.2, 30.7, 30.0, 29.9, 29.9, 29.8, 29.6, 29.5, 27.3, 23.0, 14.4. HRMS (FAB): m/z Calcd for $C_{46}H_{58}N_4S_5$ (M^+): 826.3265. Found: 826.3288. Anal. Calcd. for $C_{46}H_{58}N_4S_5$: C, 66.78; H, 7.07; N, 6.77. Found: C, 66.92; H, 7.04; N, 6.70.

*2,2′-(Benzo[c][1,2,5]thiadiazol-4,7-diyl)-4,4′,6,6′-tetra-n-hexyl-bis(4H-dithieno[3,2-b:2′,3′-d]pyrrole) (**Ic**).* The crude product was purified by flash chromatography (silica gel, 4:1 hexanes/toluene then 1:1 hexanes/toluene). The product was recrystallized from isopropanol and collected as a dark purple solid (0.659 g, 0.796 mmol, 26%). ^{1}H NMR (400 MHz, $CDCl_3$) δ 8.18 (s, 2H), 7.67 (s, 2H), 6.67 (s, 2H), 4.11 (t, J = 7.1 Hz, 4H), 2.87 (t, J = 7.6 Hz, 4H), 1.86 (quint., J = 7.1 Hz, 4H), 1.73 (quint., J = 7.5 Hz, 4H), 1.45−1.19 (m, 24H), 0.90 (t, J = 7.0 Hz, 6H), 0.87 (t, J = 7.1 Hz, 6H). ^{13}C{^{1}H} NMR (100 MHz, $CDCl_3$) δ 152.51, 145.61, 144.93, 144.42, 135.89, 125.99, 124.06, 115.52, 112.61, 111.91, 108.25, 47.15, 31.68, 31.65, 31.62, 31.43, 30.38, 28.84, 26.67, 22.61, 22.55, 14.11, 14.06. HRMS (EI): m/z Calcd for $C_{46}H_{58}N_4S_5$ (M^+): 826.3265. Found: 826.3288. Anal. Calcd. for $C_{46}H_{58}N_4S_5$: C, 66.78; H, 7.07; N, 6.77. Found: C, 66.82; H, 7.10; N, 6.69.

*2,2′-(Benzo[c][1,2,5]thiadiazol-4,7-diyl)-4,4′-di-n-dodecyl-6,6′-di-n-hexyl-bis(4H-dithieno[3,2-b:2′,3′-d]pyrrole) (**Id**).* The crude product was purified by flash chromatography (silica gel, 4:1 hexanes/toluene then 2:1 hexanes/toluene). The product was recrystallized from isopropanol and collected as a dark purple solid (0.568 g, 0.571 mmol, 38%). ^{1}H NMR (400 MHz, $CDCl_3$) δ 8.20 (s, 2H), 7.69 (s, 2H), 6.67 (s, 2H), 4.13 (t, J = 6.9 Hz, 4H), 2.87 (t, J = 7.6 Hz, 4H), 1.87 (quint., J = 6.7 Hz, 4H), 1.73 (quint., J = 7.5 Hz, 4H), 1.41−1.22 (m, 48H), 0.90 (t, J = 6.9 Hz, 6H), 0.85 (t, J = 6.8 Hz, 6H). ^{13}C{^{1}H} NMR (100 MHz, $CDCl_3$) δ 152.56, 145.65, 144.94, 144.44, 135.90, 126.05, 124.13, 115.56, 112.63, 111.94, 108.26, 47.17, 31.90, 31.67, 31.66, 31.62, 30.40, 29.64, 29.62, 29.52, 29.33, 29.24, 28.85, 26.98, 22.68, 22.61, 14.11 (two alkyl carbon resonances not observed, presumably due to overlap). HRMS (EI): m/z Calcd for $C_{58}H_{82}N_4S_5$ (M^+): 994.5143. Found: 994.5273. Anal. Calcd. for $C_{58}H_{82}N_4S_5$: C, 69.97; H, 8.30; N, 5.63. Found: C, 69.84; H, 8.40; N, 5.57.

*2,2′-(Benzene-1,4-diyl)-4,4′-di-n-hexyl-bis(4H-dithieno[3,2-b:2′,3′-d]pyrrole) (**III**).* The crude product was purified by flash chromatography (silica gel, 5:2 hexanes/CH_2Cl_2). The product was recrystallized from isopropanol and collected as small yellow−orange needles. (0.240 g, 0.399 mmol, 47%). ^{1}H NMR (400 MHz, $CDCl_3$) δ 7.63 (s, 4H), 7.25 (s, 2H), 7.13 (d, J = 5.3 Hz, 2H), 6.98 (d, J = 5.3 Hz, 2H), 4.18 (t, J = 7.1 Hz, 4H), 1.88 (quint., J = 7.1 Hz, 4H), 1.40−1.20 (m, 12H), 0.86 (t, J = 7.1 Hz, 6H). ^{13}C{^{1}H} NMR (100 MHz, $CDCl_3$) δ 145.23, 144.82, 141.03, 134.27,

125.57, 123.24, 114.94, 114.22, 110.86, 106.77, 47.38, 31.41, 30.35, 26.67, 22.50, 14.00 (one aromatic carbon resonance not observed, presumably due to overlap). HRMS (EI): *m/z* Calcd for $C_{34}H_{36}N_2S_4$ (M^+): 600.1761. Found: 600.1754. Anal. Calcd. for $C_{34}H_{36}N_2S_4$: C, 67.96; H, 6.04; N, 4.66. Found: C, 68.00; H, 6.04; N, 4.70.

General Procedure for A-D-A Triads, ***II*** *and* ***IV***. A 0.1 M solution of the appropriate DTP **6** (1 equiv) in dry THF was cooled to −78 °C under nitrogen. After 20 min, *tert*-butyllithium (2 equiv) was added dropwise and the mixture was stirred for 1 h at −78 °C. The reaction was warmed to room temperature for 10 min before returning to −78 °C. Tributyltin chloride (2.5 equiv) was added dropwise, and the mixture was allowed to warm to room temperature and stir for 3 h. The solution was then transferred into a 0.1 M THF solution of the appropriate BTD derivative **2** or **4** (2.2 equiv) also containing *trans*-dichlorobis-(triphenylphosphine)palladium; the mixture was heated to reflux for 19 h. After cooling, the reaction mixture was quenched with water, extracted with diethyl ether, and dried over anhydrous sodium sulfate. The combined ether washes were concentrated via rotary evaporation.

*2,6-Di(benzo[c][1,2,5]thiadiazol-4-yl)-4-hexyl-4H-dithieno-[3,2-b:2′,3′-d]pyrrole (****IIa****).* The crude product was purified by flash chromatography (silica gel, chloroform). The product was recrystallized from 1:1 isopropanol/ethyl acetate and collected as a dark red solid with a minor impurity (2.05 g, 3.86 mmol, 68%). A sample of the product (500 mg, 0.940 mmol) was purified by sublimation (85.4 mg, 0.161 mmol, 17%) and was used for electronic characterization. ^{1}H NMR (400 MHz, $CDCl_3$) δ 8.32 (s, 2H), 7.86 (d, J = 8.4 Hz, 2H), 7.83 (d, J = 6.8 Hz, 2H), 7.59 (dd, J = 8.6, 7.4 Hz, 2H), 4.34 (t, J = 6.8 Hz, 2H), 2.00 (quint., J = 7.2 Hz, 2H), 1.46−1.27 (m, 6H), 0.88 (t, J = 7.0 Hz, 3H). ^{13}C{^{1}H} NMR (100 MHz, $CDCl_3$) δ 155.7, 152.0, 146.4, 137.8, 129.7, 128.7, 124.2, 119.3, 115.6, 112.7, 47.4, 31.4, 30.4, 26.7, 22.5, 14.1. HRMS (EI): *m/z* Calcd for $C_{26}H_{21}N_5S_4$ (M^+): 531.0680. Found: 531.0658. Anal. Calcd. for $C_{26}H_{21}N_5S_4$: C, 58.79; H, 3.98; N, 13.17. Found: C, 58.67; H, 3.92; N, 13.14

*2,6-Di(benzo[c][1,2,5]thiadiazol-4-yl)-4-dodecyl-4H-dithieno-[3,2-b:2′,3′-d]pyrrole (****IIb****).* The crude product was purified by flash chromatography (silica gel, 2:1 chloroform/hexanes). The solvent was removed under reduced pressure. The product was recrystallized from isopropanol and collected as a dark red solid with a minor impurity (1.53 g, 2.48 mmol, 49%). A sample of the product (1.20 g, 1.95 mmol) was purified by sublimation (0.374 g, 6.49 mmol, 31%) and used for electronic characterization. ^{1}H NMR (400 MHz, $CDCl_3$) δ 8.29 (s, 2H), 7.83 (d, J = 8.8 Hz, 2H), 7.80 (d, J = 7.2 Hz, 2H), 7.57 (dd, J = 8.4, 7.2 Hz, 2H), 4.34 (t, J = 7.2 Hz, 2H), 1.98 (quint., J = 7.2 Hz, 2H), 1.42−1.32 (m, 4H), 1.30−1.10 (m, 14H), 0.82 (t, J = 7.0 Hz, 3H). ^{13}C{^{1}H} NMR (100 MHz, $CDCl_3$) δ 155.70, 155.96, 146.35, 137.77, 129.71, 128.64, 124.21, 119.32, 115.54, 112.69, 47.34, 31.85, 30.39, 29.59, 29.47, 29.28, 29.22, 26.94, 22.63, 14.08 (two alkyl carbon resonances not observed, presumably due to overlap). HRMS (EI): *m/z* Calcd for $C_{32}H_{33}N_5S_4$ (M^+): 615.1619. Found: 615.1629. Anal. Calcd. for $C_{32}H_{33}N_5S_4$: C, 62.40; H, 5.40; N, 11.37. Found: C, 62.40; H, 5.29; N, 11.51.

*4-Hexyl-2,6-bis(7-hexylbenzo[c][1,2,5]thiadiazol-4-yl)-4H-dithieno[3,2-b:2′,3′-d]pyrrole (****IIc****).* The crude product was purified by flash chromatography (silica gel, 1:2 toluene/hexane). The product was recrystallized from isopropanol with a small amount of chloroform and collected as a dark purple solid (0.818 g, 0.117 mmol, 56%). ^{1}H NMR (400 MHz, $CDCl_3$) δ 8.25 (s, 2H), 7.76 (d, J = 7.2 Hz, 2H), 7.35 (d, J = 7.3 Hz, 2H), 4.35 (t, J = 7.0 Hz, 2H), 3.11 (t, J = 7.6 Hz, 4H), 1.98 (quint., J = 7.2 Hz, 2H), 1.80 (quint., J = 7.6 Hz, 4H), 1.44−1.26 (m, 18H), 0.88 (t, J = 7.0 Hz, 6H), 0.86 (t, J = 7.3 Hz, 3H). ^{13}C{^{1}H} NMR (100 MHz, $CDCl_3$) δ 155.68, 152.25, 146.14, 137.98, 134.46, 127.64, 126.24, 124.72, 115.03, 11.86, 47.36, 32.27, 31.70, 31.45, 30.43, 29.73, 29.24, 26.68, 22.63, 22.55, 14.11, 14.07. HRMS (EI): *m/z* Calcd for $C_{38}H_{45}N_5S_4$ (M^+): 699.2558. Found: 699.2584. Anal. Calcd. for $C_{38}H_{45}N_5S_4$: C, 65.20; H, 6.48; N, 10.00. Found: C, 64.93; H, 6.53; N, 10.01.

*4-Dodecyl-2,6-bis(7-hexylbenzo[c][1,2,5]thiadiazol-4-yl)-4H-dithieno[3,2-b:2′,3′-d]pyrrole (****IId****).* The crude product was purified by flash chromatography (silica gel, 2:1 hexanes/chloroform). The product was recrystallized from isopropanol with a small amount of chloroform and collected as a dark purple solid (0.763 g, 0.972 mmol, 52%). ^{1}H NMR (400 MHz, $CDCl_3$) δ 8.22 (s, 2H), 7.73 (d, J = 7.2 Hz, 2H), 7.32 (d, J = 7.3 Hz, 2H), 4.31 (t, J = 6.9 Hz, 2H), 3.10 (t, J = 7.6 Hz, 4H), 1.96 (quint., J = 7.0 Hz, 2H), 1.79 (quint., J = 7.6 Hz, 4H), 1.42−1.18 (m, 32H), 0.88 (t, J = 7.0 Hz, 6H), 0.83 (t, J = 7.0 Hz, 3H). ^{13}C{^{1}H} NMR (100 MHz, $CDCl_3$) δ 155.64, 152.20, 146.13, 137.94, 134.38, 127.59, 126.22, 124.63, 114.99, 111.86, 47.29, 32.25, 31.87, 31.70, 30.40, 29.70, 29.61, 29.59, 29.49, 29.29, 29.25, 26.95, 22.64, 14.10 (four alkyl carbon resonances not observed, presumably due to overlap). HRMS (EI): *m/z* Calcd for $C_{44}H_{57}N_5S_4$ (M^+): 783.3968. Found: 783.3467. Anal. Calcd. for $C_{44}H_{57}N_5S_4$: C, 67.39; H, 7.33; N, 8.93. Found: C, 67.36; H, 7.34; N, 8.90.

*4-Hexyl-2,6-diphenyl-4H-dithieno[3,2-b:2′,3′-d]pyrrole (****IV****).* The crude product was purified by flash chromatography (silica gel, 5:1 hexanes/dichloromethane). The product was recrystallized from isopropanol and collected as small, yellow-orange needles. (0.246 g, 0.592 mmol, 50%). ^{1}H NMR (300 MHz, $(CD_3)_2CO$) δ 7.72 (d, J = 7.5 Hz, 4H), 7.68 (s, 2H), 7.41 (t, J = 7.4 Hz, 4H), 7.28 (t, J = 7.4 Hz, 2H), 4.38 (t, J = 6.9 Hz, 2H), 1.95 (quint., J = 6.8 Hz, 2H), 1.50−1.20 (m, 6H), 0.84 (t, J = 6.6 Hz, 3H). ^{13}C{^{1}H} NMR (75 MHz, $(CD_3)_2CO$) δ 146.24, 142.28, 136.45, 129.84, 127.97, 125.78, 108.83, 105.84, 47.67, 32.13, 31.06, 27.23, 23.21, 14.23 (two aromatic carbon resonances not observed, presumably due to overlap). HRMS (EI): *m/z* Calcd for $C_{26}H_{25}NS_2$ (M^+): 415.1428. Found: 415.1425. Anal. Calcd. for $C_{26}H_{25}NS_2$: C, 75.14; H, 6.06; N, 3.37. Found: C, 74.97; H, 5.91; N, 3.44.

■ ASSOCIATED CONTENT

Ⓢ Supporting Information. Additional characterization along with additional quantum-chemical calculation results and supporting figures. This material is available free of charge via the Internet at http://pubs.acs.org.

■ AUTHOR INFORMATION

Corresponding Author

*E-mail: seth.marder@gatech.edu.

Present Addresses

‖Indian Institute of Technology Rajasthan, Jodhpur, Rajasthan, 342011, India.

■ ACKNOWLEDGMENT

This research was financially supported by Solvay S.A. and through the STC Program of the National Science Foundation

(DMR 0120967). L.E.P. gratefully acknowledges Yulia Getmanenko for helpful discussions.

REFERENCES

(1) Facchetti, A. *Chem. Mater.* **2011**, *23*, 733–758.
(2) Bundgaard, E. *Sol. Energy Mater. Sol. Cells* **2007**, *91*, 954–985.
(3) Beaujuge, P. M.; Pisula, W.; Tsao, H. N.; Ellinger, S.; Müllen, K.; Reynolds, J. R. *J. Am. Chem. Soc.* **2009**, *131*, 7514–7515.
(4) Blouin, N.; Michaud, A.; Leclerc, M. *Adv. Mater.* **2007**, *19*, 2295–2300.
(5) Li, Y.; Zou, Y. *Adv. Mater.* **2008**, *20*, 2952–2958.
(6) Liang, Y.; Feng, D.; Wu, Y.; Tsai, S.-T.; Li, G.; Ray, C.; Yu, L. *J. Am. Chem. Soc.* **2009**, *131*, 7792–7799.
(7) Park, S. H.; Roy, A.; Beaupré, S.; Cho, S.; Coates, N.; Moon, J. S.; Moses, D.; Leclerc, M.; Lee, K.; Heeger, A. J. *Nat. Photonics* **2009**, *3*, 297–302.
(8) Peet, J.; Kim, J. Y.; Coates, N. E.; Ma, W. L.; Moses, D.; Heeger, A. J.; Bazan, G. C. *Nat. Mater.* **2007**, *6*, 497–500.
(9) Svensson, M.; Zhang, F.; Veenstra, S. C.; Verhees, W. J. H.; Hummelen, J. C.; Kroon, J. M.; Inganäs, O.; Andersson, M. R. *Adv. Mater.* **2003**, *15*, 988–991.
(10) Wang, E.; Wang, L.; Lan, L.; Luo, C.; Zhuang, W.; Peng, J.; Cao, Y. *Appl. Phys. Lett.* **2008**, *92*, 033307.
(11) Wang, J.-Y.; Hau, S. K.; Yip, H.-L.; Davies, J. A.; Chen, K.-S.; Zhang, Y.; Sun, Y.; Jen, A. K. Y. *Chem. Mater.* **2011**, *23*, 765–767.
(12) Zhang, Y.; Hau, S. K.; Yip, H.-L.; Sun, Y.; Acton, O.; Jen, A. K. Y. *Chem. Mater.* **2010**, *22*, 2696–2698.
(13) Zou, Y.; Najari, A.; Berrouard, P.; Beaupré, S.; Aïch, B. R.; Tao, Y.; Leclerc, M. *J. Am. Chem. Soc.* **2010**, *132*, 5330–5331.
(14) Zhu, Y.; Champion, R. D.; Jenekhe, S. A. *Macromolecules* **2006**, *39*, 8712–8719.
(15) Mikroyannidis, J. A.; Tsagkournos, D. V.; Sharma, S. S.; Vijay, Y. K.; Sharma, G. D. *J. Mater. Chem.* **2011**, *21*, 4679–4688.
(16) Sharma, G. D.; Balraju, P.; Mikroyannidis, J. A.; Stylianakis, M. M. *Sol. Energy Mater. Sol. Cells* **2009**, *93*, 2025–2028.
(17) Zheng, Q.; Jung, B. J.; Sun, J.; Katz, H. E. *J. Am. Chem. Soc.* **2010**, *132*, 5394–5404.
(18) Cheng, Y.-J.; Wu, J.-S.; Shih, P.-I.; Chang, C.-Y.; Jwo, P.-C.; Kao, W.-S.; Hsu, C.-S. *Chem. Mater.* **2011**, *23*, 2361–2369.
(19) Li, Z.; McNeill, C. R. *J. Appl. Phys.* **2011**, *109*, 074513.
(20) Zhou, J.; Wan, X.; Liu, Y.; Wang, F.; Long, G.; Li, C.; Chen, Y. *Macromol. Chem. Phys.* **2011**, *212*, 1109–1114.
(21) Zhang, S.; Guo, Y.; Fan, H.; Liu, Y.; Chen, H.-Y.; Yang, G.; Zhan, X.; Liu, Y.; Li, Y.; Yang, Y. *J. Polym. Sci., Part A: Polym. Chem.* **2009**, *47*, 5498–5508.
(22) Sonar, P.; Williams, E. L.; Singh, S. P.; Dodabalapur, A. *J. Mater. Chem.* **2011**, *21*, 10532–10541.
(23) Hou, J.; Chen, H.; Zhang, S.; Li, G.; Yang, Y. *J. Am. Chem. Soc.* **2008**, *130*, 16144–16145.
(24) Zhang, X.; Steckler, T. T.; Dasari, R. R.; Ohira, S.; Potscavage, W. J.; Tiwari, S. P.; Coppée, S.; Ellinger, S.; Barlow, S.; Brédas, J.-L.; et al. *J. Mater. Chem.* **2010**, *20*, 123–134.
(25) Yue, W.; Zhao, Y.; Shao, S.; Tian, H.; Xie, Z.; Geng, Y.; Wang, F. *J. Mater. Chem.* **2009**, *19*, 2199–2206.
(26) Zaumseil, J.; Sirringhaus, H. *Chem. Rev.* **2007**, *107*, 1296–1323.
(27) Bürgi, L.; Turbiez, M.; Pfeiffer, R.; Bienewald, F.; Kirner, H.-J.; Winnewisser, C. *Adv. Mater.* **2008**, *20*, 2217–2224.
(28) Gadisa, A.; Mammo, W.; Andersson, L. M.; Admassie, S.; Zhang, F.; Andersson, M. R.; Inganäs, O. *Adv. Funct. Mater.* **2007**, *17*, 3836–3842.
(29) Gwinner, M. C.; Khodabakhsh, S.; Giessen, H.; Sirringhaus, H. *Chem. Mater.* **2009**, *21*, 4425–4433.
(30) Kim, F. S.; Guo, X.; Watson, M. D.; Jenekhe, S. A. *Adv. Mater.* **2010**, *22*, 478–482.
(31) Zoombelt, A. P.; Mathijssen, S. G. J.; Turbiez, M. G. R.; Wienk, M. M.; Janssen, R. A. J. *J. Mater. Chem.* **2010**, *20*, 2240–2246.
(32) Steckler, T. T.; Zhang, X.; Hwang, J.; Honeyager, R.; Ohira, S.; Zhang, X.-H.; Grant, A.; Ellinger, S.; Odom, S. A.; Sweat, D.; et al. *J. Am. Chem. Soc.* **2009**, *131*, 2824–2926.
(33) Usta, H.; Facchetti, A.; Marks, T. J. *J. Am. Chem. Soc.* **2008**, *130*, 8580–8581.
(34) Yoon, M.; DiBenedetto, S.; Facchetti, A.; Marks, T. *J. Am. Chem. Soc.* **2005**, *127*, 1348–1349.
(35) Chesterfield, R. J.; Newman, C. R.; Pappenfus, T. M.; Ewbank, P. C.; Haukaas, M. H.; Mann, K. R.; Miller, L. L.; Frisbie, C. D. *Adv. Mater.* **2003**, *15*, 1278–1282.
(36) Zaumseil, J.; Donley, C.; Kim, J.-S.; Friend, R.; Sirringhaus, H. *Adv. Mater.* **2006**, *18*, 2708–2712.
(37) Welch, G. C.; Bazan, G. C. *J. Am. Chem. Soc.* **2011**, *133*, 4632–4644.
(38) Murphy, A.; Fréchet, J. *Chem. Rev.* **2007**, *107*, 1066–1069.
(39) Mas-Torrent, M.; Rovira, C. *Chem. Soc. Rev.* **2008**, *37*, 827–838.
(40) Jurchescu, O. D.; Baas, J.; Palstra, T. T. M. *Appl. Phys. Lett.* **2004**, *84*, 3061–3063.
(41) Ogawa, K.; Rasmussen, S. *J. Org. Chem.* **2003**, *68*, 2921–2928.
(42) Barlow, S.; Odom, S. A.; Lancaster, K.; Getmanenko, Y. A.; Mason, R.; Coropceanu, V.; Brédas, J.-L.; Marder, S. R. *J. Phys. Chem. B* **2010**, *114*, 14397–14407.
(43) Ohshita, J.; Nodono, M.; Kai, H.; Watanabe, T.; Kunai, A.; Komaguchi, K.; Shiotani, M.; Adachi, A.; Okita, K.; Harima, Y.; et al. *Organometallics* **1999**, *18*, 1453–1459.
(44) Chochos, C. L.; Choulis, S. A. *Prog. Polym. Sci.* **2011**, 1–89.
(45) Bundgaard, E.; Krebs, F. C. *Macromolecules* **2006**, *39*, 2823–2831.
(46) Horie, M.; Majewski, L. A.; Fearn, M. J.; Yu, C.-Y.; Luo, Y.; Song, A.; Saunders, B. R.; Turner, M. L. *J. Mater. Chem.* **2010**, *20*, 4347–4355.
(47) Welch, G. C.; Coffin, R.; Peet, J.; Bazan, G. C. *J. Am. Chem. Soc.* **2009**, *131*, 10802–10803.
(48) Karsten, B. P.; Bijleveld, J. C.; Viani, L.; Cornil, J.; Gierschner, J.; Janssen, R. A. J. *J. Mater. Chem.* **2009**, *19*, 5343–5350.
(49) Sonar, P.; Singh, S. P.; Leclère, P.; Surin, M.; Lazzaroni, R.; Lin, T. T.; Dodabalapur, A.; Sellinger, A. *J. Mater. Chem.* **2009**, *19*, 3228–3237.
(50) Sonar, P.; Singh, S. P.; Sudhakar, S.; Dodabalapur, A.; Sellinger, A. *Chem. Mater.* **2008**, *20*, 3184–3190.
(51) Steinberger, S.; Mishra, A.; Reinold, E.; Levichkov, J.; Uhrich, C.; Pfeiffer, M.; Bäuerle, P. *Chem. Commun.* **2011**, *47*, 1982–1984.
(52) Pilgram, K.; Zupan, M.; Skiles, R. *J. Heterocycl. Chem.* **1970**, *7*, 629–633.
(53) Gronowitz, S. *Acta Chem. Scand.* **1961**, *15*, 1393–1395.
(54) Evenson, S. J.; Rasmussen, S. C. *Org. Lett.* **2010**, *12*, 4054–4057.
(55) Mishra, S. P.; Palai, A. K.; Srivastava, R.; Kamalasanan, M. N.; Patri, M. *J. Polym. Sci., Polym. Chem.* **2009**, *47*, 6514–6525.
(56) Koeckelberghs, G.; de Cremer, L.; Vanormelingen, W.; Dehaen, W.; Verbiest, T.; Persoons, A.; Samyn, C. *Tetrahedron* **2005**, *61*, 687–691.
(57) Neutral ground-state structures at the Hartree−Fock (HF/6-31G**) level are moderately twisted for triads **I** and **II** (torsion angles ca. 22°) and further twisted for **III** and **IV** (torsion angles ca. 39°).
(58) The compounds with terminal alkyl groups, **Ic/d** and **IIc/d** show very similar orbitals to their hydrogen-terminated analogues and the frontier orbitals at the HF/6-31G** level are qualitatively similar to the DFT orbitals.
(59) Sato, T.; Hori, K.; Fujitsuka, M.; Watanabe, A.; Ito, O.; Tanaka, K. *J. Chem. Soc., Faraday Trans.* **1998**, *94*, 2355–2360.
(60) Hankache, J.; Wenger, O. S. *Chem. Rev.* **2011**, *111*, 5138–5178.
(61) Mori-Sánchez, P.; Cohen, A. J.; Yang, W. *Phys. Rev. Lett.* **2008**, *100*, 146401.
(62) Distribution of HF Mulliken charges are broadly consistent with distribution of DFT charges, see Table S2.
(63) Mo, H.; Radke, K. R.; Ogawa, K.; Heth, C. L.; Erpelding, B. T.; Rasussen, S. C. *Phys. Chem. Chem. Phys.* **2010**, *12*, 14585–14595.
(64) Silva-Junior, M. R.; Schreiber, M.; Sauer, S. P. A.; Thiel, W. *J. Chem. Phys.* **2008**, *129*, 104103.
(65) Peach, M. J. G.; Benfield, P.; Helgaker, T.; Tozer, D. J. *J. Chem. Phys.* **2008**, *128*, 044118.
(66) Although the transition energies obtained using the long-range corrected functionals are hypsochromically shifted from the experimental maxima, the calculated absorption profiles for the visible region are in good qualitative agreement and the CI descriptions of the transitions are qualitatively similar (see Tables S4 and S5 for details).

(67) Apperloo, J. J.; Groenendaal, L. B.; Verheyen, H.; Jayakannan, M.; Janssen, R. A. J.; Dkhissi, A.; Beljonne, D.; Lazzaroni, R.; Brédas, J.-L. *Chem.—Eur. J.* **2002**, *8*, 2384–2396.
(68) Yassin, A.; Leriche, P.; Roncali, J. *Macromol. Rapid Commun.* **2010**, *31*, 1467–1472.
(69) Kojima, T.; Nishida, J.-i.; Tokito, S.; Tada, H.; Yamashita, Y. *Chem. Commun.* **2007**, 1430–1432.
(70) Omer, K. M.; Ku, S.-Y.; Wong, K.-T.; Bard, A. J. *J. Am. Chem. Soc.* **2009**, *131*, 10733–10741.
(71) Watanabe, M.; Goto, K.; Shibahara, M.; Shinmyozu, T. *J. Org. Chem.* **2010**, *75*, 6104–6114.
(72) It has been suggested that an offset of 5.1 eV has a more sound theoretical basis based on the absolute potential of $FeCp_2^{+/0}$ vs vacuum (Cardona, C. M.; Li, W.; Kaifer, A. E.; Stockdale, D.; Bazan, G. C. *Adv. Mater.* **2011**, *23*, 2367–2371.).However, we have used the value of 4.8 eV for consistency with much of the literature, due to the relatively good empirical agreement obtained with solid-state UPS determination of IP in many cases and due to the measurement of a solid-state IP of 4.8 eV for a close analogue of ferrocene (D'Andrade, B.; Datta, S.; Forrest, S.; Djurovich, P.; Polikarpov, E.; Thompson, M. *Org. Electron.* **2005**, *6*, 11–20).
(73) Marcus, R. A. *Rev. Mod. Phys.* **1993**, *65*, 599–610.
(74) Malagoli, M.; Brédas, J.-L. *Chem. Phys. Lett.* **2000**, *327*, 13–17.
(75) da Silva Filho, D. A.; Coropceanu, V.; Fichou, D.; Gruhn, N. E.; Bill, T. G.; Gierschner, J.; Cornil, J.; Brédas, J.-L. *Philos. Trans. R. Soc. A: Math. Phys. Eng. Sci.* **2007**, *365*, 1435–1452.
(76) Lin, B. C.; Cheng, C. P.; You, Z.-Q.; Hsu, C.-P. *J. Am. Chem. Soc.* **2004**, *127*, 66–67.
(77) Coropceanu, V.; Malagoli, M.; da Silva Filho, D. A.; Gruhn, N. E.; Bill, T. G.; Brédas, J. L. *Phys. Rev. Lett.* **2002**, *89*, 275503.
(78) Barlow, S.; Zhang, Q.; Kaafarani, B. R.; Risko, C.; Amy, F.; Chan, C. K.; Domercq, B.; Starikova, Z. A.; Antipin, M. Y.; Timofeeva, T. V.; et al. *Chem.—Eur. J.* **2007**, *13*, 3537.
(79) Connelly, N.; Geiger, W. *Chem. Rev.* **1996**, *96*, 877–910.
(80) Guay, J.; Kasai, P.; Diaz, A.; Wu, R.; Tour, J.; Dao, L. *Chem. Mater.* **1992**, *4*, 1097–1105.
(81) Fichou, D.; Horowitz, G.; Xu, B.; Garnier, F. *Synth. Met.* **1990**, *39*, 243–259.
(82) Fujitsuka, M.; Sato, T.; Sezaki, F.; Tanaka, K.; Watanabe, A.; Ito, O. *J. Chem. Soc., Faraday Trans.* **1998**, *94*, 3331–3337.
(83) Graf, D.; Duan, R.; Campbell, J.; Miller, L.; Mann, K. *J. Am. Chem. Soc.* **1997**, *119*, 5888–5899.
(84) Polander, L. E.; Tiwari, S. P.; Pandey, L.; Seifried, B. M.; Zhang, Q.; Barlow, S.; Risko, C.; Brédas, J.-L.; Kippelen, B.; Marder, S. R. *Chem. Mater.* **2011**, *23*, 3408–3410.
(85) From the estimated solid-state IPs and excited-state energies, E_{op}, of Table 3, and using a value of −3.8 eV for the solid-state EA of PCBM (Guan, Z.-L.; Kim, J. B.; Wang, H.; Jaye, C.; Fischer, D. A.; Loo, Y.-L.; Kahn, A. *Org. Electron.* **2010**, *11*, 1779), a commonly used acceptor in photovoltaic studies, one can estimate ΔG for electron transfer from the photoexcited dyads to PCBM to be in the range −0.7 to −0.8 eV.
(86) Becke, A. D. *Phys. Rev. A* **1988**, *38*, 3098–3100.
(87) Becke, A. D. *J. Chem. Phys.* **1993**, *98*, 5648–5652.
(88) Lee, C.; Yang, W.; Parr, R. G. *Phys. Rev. B* **1988**, *37*, 785–789.
(89) Hariharan, P. C.; Pople, J. A. *Theor. Chim. Acta* **1973**, *28*, 213–222.
(90) Francl, M. M.; Pietro, W. J.; Hehre, W. J.; Binkley, J. S.; Gordon, M. S.; DeFrees, D. J.; Pople, J. A. *J. Chem. Phys.* **1982**, *77*, 3654–3665.
(91) Rassolov, V. A.; Pople, J. A.; Ratner, M. A.; Windus, T. L. *J. Chem. Phys.* **1998**, *109*, 1223–1229.
(92) Pacchioni, G.; Frigoli, F.; Ricci, D.; Weil, J. A. *Phys. Rev. B* **2000**, *63*, 054102.
(93) Chai, J.; Head-Gordon, M. *J. Chem. Phys.* **2008**, *128*, 084106.
(94) Dreuw, A.; Head-Gordon, M. *J. Am. Chem. Soc.* **2004**, *126*, 4007–4016.
(95) Yanai, T.; Tew, D. P.; Handy, N. C. *Chem. Phys. Lett.* **2004**, *393*, 51–57.
(96) Scalmani, G.; Frisch, M. J. *J. Chem. Phys.* **2010**, *132*, 114110.
(97) Frisch, M. J. T., G. W.; Schlegel, H. B.; Scuseria, G. E.; Robb, M. A.; Cheeseman, J. R.; Montgomery, Jr., J. A.; Vreven, T.; Kudin, K. N.; Burant, J. C.; Millam, J. M.; et al. *Gaussian 03*, revision E.01; Gaussian, Inc.: Wallingford CT, 2004.
(98) Frisch, M. J. T., G. W.; Schlegel, H. B.; Scuseria, G. E.; Robb, M. A.; Cheeseman, J. R.; Scalmani, G.; Barone, V.; Mennucci, B.; Petersson, G. A.; Nakatsuji, H.; et al. *Gaussian 09*, revision A.02; Gaussian Inc.: Wallingford CT, 2009.